

Amphibole megacrysts as a probe into the deep plumbing system of Merapi volcano, Central Java, Indonesia

Stefan T. M. Peters^{1,2} · Valentin R. Troll³ · Franz A. Weis⁴ · Luigi Dallai⁵ · Jane P. Chadwick^{2,6} · Bernhard Schulz⁷

Received: 15 August 2016 / Accepted: 21 February 2017 / Published online: 16 March 2017
© Springer-Verlag Berlin Heidelberg 2017

Abstract Amphibole has been discussed to potentially represent an important phase during early chemical evolution of arc magmas, but is not commonly observed in eruptive arc rocks. Here, we present an in-depth study of metastable calcic amphibole megacrysts in basaltic andesites of Merapi volcano, Indonesia. Radiogenic Sr and Nd isotope compositions of the amphibole megacrysts overlap with the host rock range, indicating that they represent antecrysts to the host magmas rather than xenocrysts. Amphibole-based barometry suggests that the megacrysts crystallised

at pressures of >500 MPa, i.e., in the mid- to lower crust beneath Merapi. Rare-earth element concentrations, in turn, require the absence of magmatic garnet in the Merapi feeding system and, therefore, place an uppermost limit for the pressure of amphibole crystallisation at ca. 800 MPa. The host magmas of the megacrysts seem to have fractionated significant amounts of amphibole and/or clinopyroxene, because of their low Dy/Yb ratios relative to the estimated compositions of the parent magmas to the megacrysts. The megacrysts' parent magmas at depth may thus have evolved by amphibole fractionation, in line with apparently coupled variations of trace element ratios in the megacrysts, such as e.g., decreasing Zr/Hf with Dy/Yb. Moreover, the Th/U ratios of the amphibole megacrysts decrease with increasing Dy/Yb and are lower than Th/U ratios in the basaltic andesite host rocks. Uranium in the megacrysts' parent magmas, therefore, may have occurred predominantly in the tetravalent state, suggesting that magmatic fO_2 in the Merapi plumbing system increased from below the FMQ buffer in the mid-to-lower crust to 0.6–2.2 log units above it in the near surface environment. In addition, some of the amphibole megacrysts experienced dehydrogenation (H_2 loss) and/or dehydration (H_2O loss), as recorded by their variable H_2O contents and D/H and Fe^{3+}/Fe^{2+} ratios, and the release of these volatile species into the shallow plumbing system may facilitate Merapi's often erratic eruptive behaviour.

Communicated by Othmar Müntener.

Electronic supplementary material The online version of this article (doi:10.1007/s00410-017-1338-0) contains supplementary material, which is available to authorized users.

✉ Stefan T. M. Peters
s.peters@geo.uni-goettingen.de

- 1 Abteilung Isotopengeologie, Geowissenschaftliches Zentrum der Georg-August-Universität Göttingen, Goldschmidtstrasse 1, 37077 Göttingen, Germany
- 2 Faculteit der Aard- en Levenswetenschappen, Vrije Universiteit Amsterdam, De Boelelaan 1085, 1081 HV Amsterdam, The Netherlands
- 3 Department of Earth Sciences, Section for Mineralogy, Petrology and Tectonics, Uppsala University, Villavägen 16, SE 752 36 Uppsala, Sweden
- 4 Department of Geosciences, Swedish Museum of Natural History, 114 Stockholm, Sweden
- 5 CNR-Istituto di Geoscienze e Georisorse, Via Moruzzi 1, 56124 Pisa, Italy
- 6 Science Gallery, Trinity College Dublin, Pearse Street, Dublin, Ireland
- 7 Institut für Mineralogie, TU Bergakademie Freiberg, Brennhausgasse 14, 09599 Freiberg, Saxony, Germany

Keywords Magmatic differentiation · Rare-earth elements · Arc magmas · Barometry · Dehydrogenation · Dehydration

Introduction

The role of amphibole in the chemical evolution of arc magmas

Fractional crystallisation of amphibole has long been considered an important factor during the evolution of arc magmas (e.g., Cawthorn and O'Hara 1976; Ringwood 1974; Foden and Green 1992; Romick et al. 1992; Rutherford and Hill 1993). Amphibole is commonly present in exhumed deep crustal suites derived from island arcs, where it forms a cumulate phase in gabbros, diorites, and amphibolites (e.g., Beard 1986; DeBari and Coleman 1989, LaPierre et al. 1992; Larocque and Canil 2010). However, it is rarely found as a major mineral constituent in arc lavas, although trends of decreasing Dy/Yb and increasing Yb/La with SiO₂ suggest that many arc lavas have likely fractionated amphibole during petrogenesis (e.g., MacPherson et al. 2006; Davidson et al. 2007). In addition, amphibole bearing xenoliths are occasionally found in arc lavas (e.g., Conrad and Kay 1984; Debari et al. 1987; Camus et al. 2000; Turner et al. 2003; Chadwick et al. 2013), suggesting that the deep levels of modern island arcs may, indeed, bear similarities to their exhumed plutonic counterparts. Amphibole megacrysts have been reported from a small number of arc volcanoes and then generally show chemical disequilibrium with their host magmas (e.g., Sigurdsson and Shepherd 1974; Downes et al. 1995; Murphy et al. 1998; Rooney et al. 2011; Krawczynski et al. 2012). It has been conjectured that such amphibole megacrysts formed in the deeper parts of the magmatic systems, and thus may record differentiation processes that occurred during the earlier stages of magma evolution (e.g., Kiss et al. 2014). Moreover, resorption of disequilibrium amphibole could have temporarily added volatile species to the magmatic systems of these volcanoes, which could have affected their eruptive behaviour (e.g., Feeley and Sharp 1996; Davidson et al. 2007). Notably, fractional crystallisation of amphibole has been suggested to control major and trace element evolutions of basaltic andesite magmas from Merapi volcano, Indonesia (Wulaningsih et al. 2013) and amphibole megacrysts are frequently present in the recent deposits of this volcano (Chadwick et al. 2013; Costa et al. 2013; Preece et al. 2013; Nadeau et al. 2013; Erdmann et al. 2014). Here, we focus on the origin of the Merapi amphibole megacrysts and report on their major and trace element compositions, petrography, their Sr and Nd isotope compositions and their Fe³⁺/Fe²⁺ ratios, as well as their H₂O content and H isotope compositions. The depths at which the amphibole megacrysts formed are then discussed based on geobarometric model calculations, and finally, trace element concentrations in

the amphibole megacrysts are used to assess the role of deep amphibole fractionation in the evolution of recent Merapi magmas.

Geochemistry of Merapi magmas

Merapi volcano is the youngest of a cross-island chain of four stratovolcanoes in Central Java (van Bemmelen 1949). The recent activity at Merapi is characterized by the formation and subsequent collapse of lava domes, resulting in the frequent deposition of block-and-ash flows on the upper slopes of the volcano (e.g., Voight et al. 2000; Gertisser et al. 2012), but occasionally, larger explosive events occur, as, e.g., the most recent eruption in 2010 (Surono et al. 2012). The lower flanks of Merapi expose Holocene pyroclastic deposits, which are underlain by basaltic andesite lava flows that are the product of an older volcanic structure (Old Merapi, e.g., van Bemmelen 1949; Newhall et al. 2000) and indicate that volcanism at Merapi commenced $\geq 40,000$ years ago (Camus et al. 2000; Berthommier et al. 1990; Newhall et al. 2000).

The Holocene deposits of Merapi are dominantly basaltic andesites with a marked transition from a medium- to a high-*K* composition at ~ 1900 BP (Gertisser and Keller 2003). The high-*K* series is commonly referred to as basaltic andesites (e.g., Gertisser and Keller 2003; Gertisser et al. 2012), but classify as basaltic trachy-andesites in the TAS diagram (cf., Le Maitre 2002). Igneous and meta-sedimentary inclusions in Merapi lavas show a wide range of textures and compositions, indicating a complex sub-volcanic plumbing system with likely multiple magma chambers and pockets distributed through the crust (Chadwick et al. 2013; Troll et al. 2013). These magma pockets appear linked into a steady-state supply network that is able to maintain overall compositional and textural stability for prolonged periods of time (e.g., van der Zwan et al. 2013). In addition, elevated ⁸⁷Sr/⁸⁶Sr ratios and $\delta^{18}\text{O}$ values in plagioclase phenocrysts, as well as temporarily elevated $\delta^{13}\text{C}$ in fumarole gases reflect an element of assimilation of carbonates in the upper sediment-rich crust (Chadwick et al. 2007; Troll et al. 2012, 2013; Borisova et al. 2016).

Amphibole megacrysts are known from recent Merapi eruptions (e.g., 1994, 1998, 2006, and 2010) and are thought of as xenocrystic and/or antecrystic in origin (Chadwick et al. 2013; Costa et al. 2013; Preece et al. 2013; Nadeau et al. 2013; Erdmann et al. 2014). Erdmann et al. (2014) reported two distinct populations of amphibole megacrysts from the 2010 eruption. They interpreted megacrysts up to ~ 2 cm with low SiO₂ and high Al₂O₃ as xenocrysts derived from mafic cumulates (cf., Chadwick et al. 2013; Nadeau et al. 2013; Preece et al. 2013), while megacrysts with respectively high and low SiO₂ and Al₂O₃ are considered xenocrystic and/or antecrystic in origin, e.g.,

from crystal mushes or fully crystallised magma pockets. Costa et al. (2013) noticed that amphibole megacrysts from the 2006 eruption have breakdown rims, whereas those of the 2010 eruption are pristine, possibly indicating a larger contribution of a deep, volatile rich magma to the 2010 eruption. Here, we complement these recent advances with the first in-depth investigation of amphibole megacrysts from the 1998 eruption deposits that contained exceptionally large amphibole crystals of up to 8 cm across. In addition, we present hydrogen isotope analyses of amphibole megacrysts from the 1998 as well as the 1994 and 2006 eruptions to help put the 1998 data into context.

Materials and methods

Samples, petrography, and major element analyses

Samples of basaltic andesite from block-and-ash flow deposits of the 1994 and 1998 eruptions were collected in 2002 on the southwest flank of Merapi, some 5–8 km from the summit (see Chadwick et al. 2007, 2013; Troll et al. 2013) and the 2006 eruptives were sampled in Kaliatem village, located on the southern flank, ~6 km from the volcano's summit (Donoghue et al. 2009). Carbon-coated thick-sections (120 μm thick) of 16 amphibole megacrysts were used for petrographic characterisation and in situ analysis of major elements (Si, Al, Mg, Fe, Ti, Ca, Na, and K) by electron microprobe (EMP) analysis on a JEOL JXA-8800M instrument at VU University Amsterdam (VU), The Netherlands, and on a JEOL JXA-8200 located at the Department of Applied Mineralogy, Geozentrum Nordbayern University of Erlangen-Nuernberg (GZN), Germany. Measurement conditions were 15 kV acceleration voltage and 10 nA probe current. The beam diameter was set to 1 μm for all elements except for Na, which was measured with a widened beam of ~10 μm in diameter.

Trace elements and Sr–Nd isotope analyses

Six large amphibole megacrysts without visible weathering were selected for trace element and isotope analyses, and carefully separated from the rock matrix by hand with a small chisel. These are different amphibole crystals than those that were analysed by electron microprobe. After ultrasonic cleaning in ultrapure water, the six selected crystals were each crushed, sieved, handpicked, and digested in a concentrated HF–HNO₃ mixture at 120 °C. After digestion, aliquots were taken for separation of Sr and Nd by ion exchange chromatography (after Pin et al. 1994). The solution remaining after aliquotation was analysed for trace element concentrations with inductively coupled plasma mass spectrometry (ICPMS) on a Quadrupole ThermoFischer

X-Series-II machine at VU University Amsterdam. Trace element concentrations in the samples were determined relative to USGS reference materials BCR-2 and BHVO-2 using a method modified after Eggins et al. (1997) to correct for instrumental drift. Analytical precisions for this method were typically $\leq 5\%$, and all are $\leq 10\%$ based on repeated analyses of the reference materials.

Strontium and Nd isotope ratios were determined by thermal ionisation mass spectrometry (TIMS) on a Finnigan MAT 262 mass spectrometer in the dynamic mode at VU University Amsterdam. For Sr isotope analysis, the NIST SRM 987 standard gave stable results before and after measurements with average $^{87}\text{Sr}/^{86}\text{Sr} = 0.710217 \pm 8$ ($n=5$), slightly lower than other labs (e.g., $^{87}\text{Sr}/^{86}\text{Sr} = 0.710248 \pm 23$; Thirlwall 1991, $^{87}\text{Sr}/^{86}\text{Sr} = 0.710256 \pm 16$; Raczek et al. 2003) but within uncertainty identical to the NIST-recommended value ($^{87}\text{Sr}/^{86}\text{Sr} = 0.71034 \pm 0.00026$). Instrumental mass bias was corrected using $^{86}\text{Sr}/^{88}\text{Sr} = 0.1194$. For Nd isotope analysis, the in-house standard CIGO (Centrum Isotopen Geologisch Onderzoek) was used that was prepared in 1985 from Nd₂O₃ obtained from Vitron, Germany, and calibrated against the La Jolla international standard (Davies et al. 2006). Our average $^{143}\text{Nd}/^{144}\text{Nd} = 0.511342 \pm 10$ ($n=5$) is in excellent agreement with the calibrated value $^{143}\text{Nd}/^{144}\text{Nd} = 0.511342 \pm 7$, and also agrees with other previous studies (e.g., Meyer et al. 2011; Koornneef et al. 2013, 2014; Klaver et al. 2015). For correction of the instrumental mass bias, the reference ratio $^{146}\text{Nd}/^{144}\text{Nd} = 0.7219$ was used.

H isotope compositions

Samples were obtained by drilling amphibole megacrysts using a Dremel® professional drill. These megacrysts are different samples than the megacrysts that had been analysed by microprobe, ICPMS, and TIMS. The retrieved powders were wrapped in silver capsules and combusted at 1450 °C in a reducing atmosphere following the procedure by Sharp et al. (2001). The hydrogen isotope analyses were performed at the CNR institute of Geosciences and Earth Resources, Pisa, using a ThermoFisher TC/EA on line with a Delta XP IRMS. All δD data are reported in the conventional “ δ -notation”, i.e., the deviation of D/H in the sample relative to VSMOW, in per mill. The precisions of the reported D/H ratios are $\pm 3\%$. At least two measurements were performed for each sample. The measured δD values were compared with those of internal standards and calibrated relative to NBS-30 ($\delta D = 65.7\%$; Hut 1987). A calibration curve was obtained with different hydrous silicate internal standards that range in composition from +160 to –40%.

H₂O concentrations

Selected parts of six megacrysts that had previously been used for H isotope analyses were crushed to obtain loose crystal fragments ($\geq 300 \mu\text{m}$) suitable for Fourier transform infrared spectroscopy (FTIR) analysis. These were handpicked under a binocular microscope and individual crystal fragments were then mounted in thermoplastic resin for further processing. With the help of crystal morphology (e.g., cleavage planes) and optical microscopy (extinction angles), the selected crystal fragments ($n=13$) were oriented along their crystallographic c -axis and their (010) crystal faces, on which the directions of the main refractive indices (α and γ) occur. Various particle size-grades of Al₂O₃-grinding paper were used to thin and polish the oriented crystal fragments to a thickness between 25 and 35 μm on the (010) crystal face. Polarized FTIR spectra in the range 2000–5000 cm^{-1} were then acquired on the oriented amphibole crystal pieces along the directions of the main refractive indices α and γ to obtain the total absorbance (A), which for amphibole corresponds to $A_{\text{total}}=A_{\alpha}+A_{\gamma}$ as A_{β} is approximately zero (Skogby and Rossman 1991). The polished crystal fragments were measured at the Swedish Museum of Natural History, Stockholm, using a Bruker Hyperion 2000 IR-microscope equipped with a NIR source (halogen lamp), a CaF₂ beam-splitter, a ZnS polarizer, and an InSb detector. Cracks and inclusions in the crystals were avoided by applying small apertures ($\sim 100 \mu\text{m}$) for masking during analysis. For each individual spectrum, 128 scans were performed and averaged. The obtained spectra were baseline corrected by a polynomial function and the individual OH bands were fitted with the software PeakFit and used for further calculations. The corresponding water contents were then calculated using the wavenumber-dependent calibration function established by Skogby and Rossman (1991), but were corrected by a factor of 10 compared to the original publication (see Stalder et al. 2012). The measurement precisions of the water contents are governed by baseline corrections and measurements of the crystal thicknesses. Based on the quality of the spectra and the large sizes of the crystal pieces, the measurement precisions are better than $\pm 10\%$ for all samples. The accuracy of the absolute water concentrations may additionally be affected by the uncertainty of the absorption coefficients (cf., Skogby and Rossman 1991). For the absolute water concentrations, we, therefore, estimate a maximum uncertainty of $\pm 20\%$.

Oxidation states of Fe

The oxidation states of Fe were determined using Mössbauer spectroscopy at the National History Museum in Stockholm in the same samples in which D/H ratios and

H₂O wt% had been measured. To obtain a sample average for different valence states, powdered crystal separates were analysed with a ⁵⁷Co standard source (active diameter 5.0 mm). In addition, selected parts of the crystals on which the H isotope compositions had been measured were analysed using a point source (active diameter 0.5 mm) to better compare the results with the hydrogen isotope data of those particular samples. Several powdered crystal pieces (10 mg in total) from individual rock samples were mixed and ground with acrylic resin and pressed to a thin disc under mild heat (150 °C) for analysis with the standard source. In addition, pieces from selected areas on the crystal for analysis with the point source were powdered, mixed, and ground with thermoplastic resin, and formed into a $\sim 1 \text{ mm}^3$ cylinder that was mounted on a strip of tape. The Mössbauer measurements were performed at incident angles of 90° and 54.7° to the γ -rays for the point and the standard source, respectively. All obtained spectra were calibrated against an α -Fe foil, folded, and reduced from 1024 to 512 channels. The spectra were fitted with the Mössbauer spectral analysis software MossA (cf., Prescher et al. 2012). During the fitting process, two doublets each were assigned to Fe²⁺ and Fe³⁺ in the octahedral positions. From the area of the doublets, the percentage of each oxidation state relative to the total iron content of the sample was obtained, assuming similar recoil-free fractions for Fe²⁺ and Fe³⁺. The estimated analytical error for the obtained Fe^{m+}/Fe_{tot} ratios is $\pm 1\%$.

Results

Petrography and EMP data

Examples of Merapi amphibole megacrysts in hand specimens are shown in Fig. 1a and b. Strong reaction zones are generally present as coronas around the crystal and within cracks (Fig. 1c, e, f). Typical minerals in these reaction zones are clinopyroxene, plagioclase, and spinel, with lesser apatite, K -feldspar, and rare anhydrite. Plagioclase in the reaction zones is dominated by two distinct compositions, namely bytownite-anorthite (An_{~90}) and labradorite (An_{40–60}), and often shows internal zoning. Spinel in the reaction zones is titanomagnetite and shows frequently lamellae of ilmenite, which has been ascribed to high-temperature oxidation (Ozima and Larson 1970). Glass is found in many reaction zones, particularly in cracks through the crystals, and occasionally occurs together with high-Mg olivine. This combination is proposed to result from incongruent partial melting of amphibole due to decompression (e.g., Foden and Green 1992). Exsolution of amphibole is observed for a portion of the megacrysts and these are typically rich in melt and fluid inclusions (e.g., Fig. 1c). Rarer

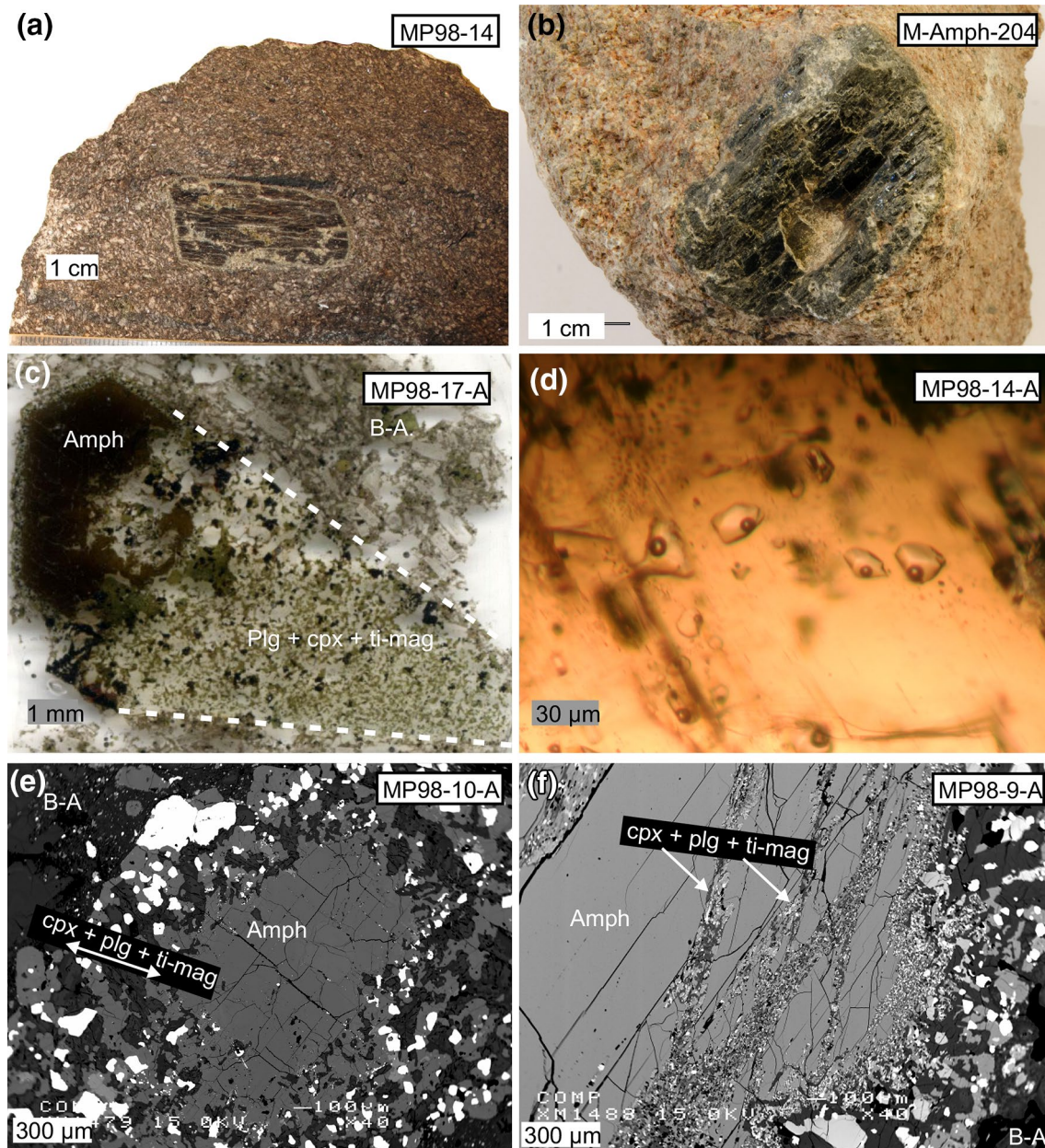


Fig. 1 Amphibole megacrysts in Merapi high-*K* basaltic andesite (1998 eruption). **a** and **b** show hand specimens. **c** Thin-section scan of an amphibole megacryst that is partially recrystallised. *Note* that the amphibole crystal shape is preserved (*dashed lines*) by the reactant phases. **d** Thin-section photograph showing fluid inclusions in amphibole. **e** Back scattered electron (BSE) image of a single amphi-

bole crystal with pronounced reaction rim at the contact with the host magma. **f** BSE image of amphibole that is partially recrystallised along crystal cracks. *Amph* amphibole, *cpx* clinopyroxene, *plg* plagioclase, *ti-mag* titanomagnetite; *B-A* basaltic andesite host magma. *Sample numbers* are indicated for each sample

crystalline inclusions in the amphibole megacrysts include clinopyroxene and opaque oxides. On occasion, the amphibole megacrysts occur together with clinopyroxene-spinel rich clots.

Representative EMP analyses are shown in Table 1, whereas the complete EMP data set ($n_{\text{total}}=205$) is provided in the supplementary materials (Appendix 1). There are no obvious differences between the EMP data from VU

and GZN. All analysed amphibole megacrysts ($n=16$) are calcic amphibole and classify either as pargasite or magnesiohastingsite, which depends on the normalisation scheme for the major cations to calculate amphibole formulas (see “Discussion”). For simplicity, we shall continue to refer to the megacrysts as “amphibole”. Amphibole compositions in the vicinity of reaction zones are typically higher in SiO_2 , TiO_2 , MnO , MgO , and Na_2O but lower in Al_2O_3 ,

Table 1 Representative EMP analyses of amphibole [wt%]

Amphibole type	MP98-2-A ^a		MP98-9A ^a		MP98-10-A ^a		MP98-13-A ^a		MP98-13-B ^a		MP98-14-A ^a	
	Primary	Primary	Primary	React. zone	Primary	React. zone	Primary	React. zone	Primary	React. zone	Primary	React. zone
SiO ₂	41.03	39.93	40.89	43.21	40.12	40.10	42.10	41.30	41.80			
TiO ₂	1.85	1.89	2.07	2.70	2.10	2.00	2.82	1.61	2.54			
Al ₂ O ₃	14.40	14.77	14.84	11.37	14.93	14.60	11.60	14.54	12.11			
Cr ₂ O ₃	n.d.	n.d.	n.d.	n.d.	n.d.	n.d.	n.d.	n.d.	n.d.			
FeO	10.26	10.08	11.22	13.64	11.23	11.44	11.75	10.79	12.09			
MnO	n.d.	n.d.	n.d.	n.d.	n.d.	n.d.	n.d.	n.d.	n.d.			
MgO	14.28	13.92	13.28	12.88	13.11	13.14	13.44	14.57	14.08			
CaO	12.08	12.36	12.35	10.94	12.42	12.29	11.24	12.14	11.63			
Na ₂ O	2.32	2.12	2.19	2.39	2.45	2.30	2.83	2.61	2.75			
K ₂ O	1.29	1.31	1.59	1.35	1.09	1.14	1.01	1.23	1.06			
Total	97.50	96.38	98.42	98.49	97.45	97.01	96.78	98.79	98.05			
Amphibole type	MP98-15-A ^a		MP98-15-B ^a		MP98-16-A ^a	MP98-101-A ^b		MP98-105-A ^b				
	Primary	React. zone	Primary	React. zone		Primary	React. zone	Primary	React. zone			
SiO ₂	41.37	43.59	40.75	42.03	40.89	38.75	38.95	40.38	40.56			
TiO ₂	1.99	1.95	2.66	3.05	1.88	1.92	2.08	2.02	3.55			
Al ₂ O ₃	14.06	12.01	14.39	12.58	14.82	13.79	13.60	12.71	11.18			
Cr ₂ O ₃	n.d.	n.d.	n.d.	n.d.	n.d.	<0.01	<0.01	<0.01	<0.01			
FeO	10.98	11.60	13.42	13.66	11.13	12.74	11.64	10.65	11.16			
MnO	n.d.	n.d.	n.d.	n.d.	n.d.	0.13	0.09	0.08	0.09			
MgO	14.38	14.78	12.85	13.11	13.59	13.16	13.58	14.80	14.42			
CaO	12.02	11.46	11.86	11.30	12.30	12.45	12.54	12.16	12.05			
Na ₂ O	2.41	2.59	2.56	2.72	2.40	2.25	2.13	2.43	2.71			
K ₂ O	1.57	1.16	1.14	1.09	1.48	1.20	1.12	1.08	0.99			
Total	98.78	99.13	99.61	99.54	98.48	96.39	95.73	96.32	96.72			
Amphibole type	MP98-105-B ^b			MP98Plfx-A ^b	Merap1-A ^b		Merap1-B ^b		Merap2-A ^b			
	Primary	Primary	React. zone		Primary	React. zone	Primary	React. zone	Primary	React. zone		
SiO ₂	40.42	40.16	40.48	41.30	40.17	42.12	39.52	39.33	40.71	44.36		
TiO ₂	1.99	1.99	2.64	1.70	2.02	3.22	1.97	3.01	1.75	1.53		
Al ₂ O ₃	13.03	12.65	11.43	13.69	14.46	11.36	14.87	13.84	13.49	10.19		
Cr ₂ O ₃	<0.01	<0.01	<0.01	0.02	0.03	<0.01	<0.01	0.01	0.06	0.01		
FeO	11.15	11.98	11.77	9.82	11.90	11.95	12.03	12.07	9.58	9.57		
MnO	0.06	0.13	0.12	0.09	0.13	0.29	0.15	0.33	0.11	0.13		
MgO	14.31	14.56	14.38	14.98	13.05	13.62	13.05	12.72	14.63	15.71		
CaO	12.17	11.98	11.77	12.26	12.19	11.08	12.12	11.75	12.13	11.25		
Na ₂ O	2.73	2.54	2.51	2.22	2.28	2.51	2.25	2.44	2.09	2.57		
K ₂ O	1.05	0.91	1.03	1.42	1.19	1.03	1.14	1.09	1.48	0.80		
Total	96.90	96.90	96.14	97.50	97.41	97.17	97.10	96.58	96.02	96.11		

^aMeasurements performed on a JEOL JXA-8800M machine (VU University Amsterdam)

^bMeasurements performed a JEOL JXA-8200 machine (University of Erlangen-Nuernberg)

CaO, and K₂O compared to parts of the crystals that are more distant to the reaction fronts. This relationship implies partial recrystallisation, during which the outer crystal lost Al, Ca, and K. The minerals in the reaction zones are enriched in these elements [e.g., apatite, anhydrite (Ca), *K*-feldspar (K), and titanomagnetite (Al)], and

the compositions of these reactants thus appear to complement the recrystallised parts of the amphibole crystals. Only one distinct population of amphibole megacrysts was observed in our samples from the 1994 and 1998 eruptions, unlike the two populations that were reported for samples from the 2010 eruption (Erdmann et al. 2014). Compared

to megacrysts from the 2010 eruption, the compositions, sizes, and textures of the amphibole megacrysts from the 1994 and 1998 eruptions appear most similar to the cumulate “M1” megacrysts of Erdmann et al. (2014), with the exceptions that megacrysts from the 1994 and 1998 eruptions are larger (up to ~8 cm) and that significant internal zoning is absent.

Trace elements and Sr–Nd isotope ratios

Trace element concentrations and $^{87}\text{Sr}/^{86}\text{Sr}$ and $^{147}\text{Nd}/^{144}\text{Nd}$ isotope ratios of selected amphibole megacrysts ($n=6$) are listed in Table 2. Most trace elements are less abundant in the amphibole megacrysts than in the basaltic andesite host magmas (Gertisser and Keller 2003), but some of the REE in the middle mass range display higher or similar concentrations. A plot of trace

element concentrations in the amphibole megacrysts relative to the basaltic andesite host rocks is presented in the online supplementary materials (Appendix 2). Niobium, Ta, Zr, and Hf have on average lower concentrations in amphibole than in the basaltic andesite, but the opposite is the case for Ti. However, Nb and Ta concentrations are variable, and appear enriched in two amphibole crystals relative to the basaltic andesite. These variable Nb and Ta concentrations likely reflect variable abundances in the amphibole megacrysts of micro-inclusions with high concentrations of these elements, e.g., Fe–Ti oxide inclusions, and are not considered fully representative for the amphibole megacrysts’ compositions. The Sr and Nd isotope ratios of the amphibole megacrysts plot roughly in the same range as the basaltic andesites from the high-*K* magma series (Fig. 2), although $^{87}\text{Sr}/^{86}\text{Sr}$ ratios are slightly less radiogenic than the data of the available

Table 2 Trace elements concentrations [ppm] and Sr–Nd isotope compositions (amphibole)

Sample	MP98-1-A	MP98-1-B	MP98-2-B	MP98-5-B	MP98-6-A	MP98-8
Rb	6.61	5.19	7.02	5.07	5.12	5.69
Ba	174	231	223	194	234	190
Th	0.1	0.12	0.09	0.27	0.13	0.36
U	0.39	0.031	0.027	0.077	0.031	0.086
Nb	0.43	0.73	0.82	1.04	0.75	0.86
Ta	0.24	0.11	0.08	2.55	0.21	0.33
La	1.26	1.92	1.7	1.92	1.95	2.27
Ce	4.5	7	6.4	6.7	7	7.1
Pb	1.1	1.14	0.58	0.9	1.1	7.1
Pr	0.93	1.43	1.35	1.32	1.44	1.36
Mo	0.026	0.022	0.009	0.023	0.024	0.014
Sr	280	366	410	340	364	304
Nd	5.9	8.9	8.8	8.2	9.06	8.1
Sm	2.51	3.57	3.71	3.15	3.49	3.13
Zr	13.1	22.5	21.4	22.8	22.3	21
Hf	0.71	1.16	1.12	1.08	1.13	0.94
Eu	0.9	1.23	1.27	1.12	1.18	1.06
Ti	12120	12774	16891	12109	12951	11428
Gd	3.13	4.42	4.82	4.16	4.45	3.82
Tb	0.5	0.68	0.75	0.66	0.68	0.615
Dy	3	4.23	4.64	4.11	4.2	3.72
Ho	0.55	0.8	0.86	0.8	0.842	0.736
Er	1.52	2.17	2.28	2.04	2.17	1.95
Tm	0.198	0.291	0.307	0.264	0.292	0.263
Yb	1.09	1.65	1.67	1.55	1.63	1.55
Lu	0.148	0.224	0.227	0.217	0.224	0.211
$^{87}\text{Sr}/^{86}\text{Sr}$	0.705507 (9)	0.705690 (10)	0.705569 (9)	0.705609 (9)	0.705566 (9)	0.705459 (10)
$^{143}\text{Nd}/^{144}\text{Nd}$	0.512710 (11)	0.512707 (9)	0.512712 (10)	0.512701 (16)	0.512736 (8)	0.512737 (9)

Trace element data are given at the $\leq 10\%$ uncertainty level. Measurement precisions (2 S.E.) of the isotope ratios in ppm are given in *brackets*. The external reproducibility of $^{87}\text{Sr}/^{86}\text{Sr}$ and $^{143}\text{Nd}/^{144}\text{Nd}$ in standard reference materials that were analysed during the same analytical session was 8 and 10 ppm, respectively (2σ , $n=5$ each)

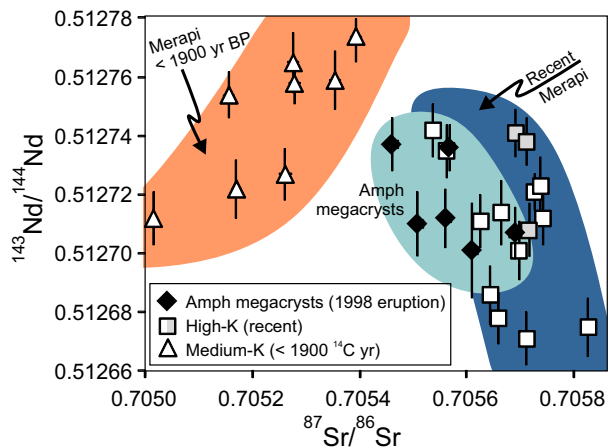


Fig. 2 Sr–Nd isotope compositions of amphibole megacrysts relative to the older medium-*K* and the recent high-*K* Merapi basaltic andesite lavas of Gertisser and Keller (2003). The Nd isotope compositions of amphibole megacrysts overlap with the least radiogenic samples of the recent high-*K* basaltic andesite series, whereas Sr isotope compositions of some amphibole megacrysts are less radiogenic than the high-*K* basaltic andesite magmas. *Black, grey and white symbols* correspond to data from this work, Gertisser and Keller (2003) and Jolis (2013) respectively

whole rock suite (e.g., Gertisser and Keller 2003; Chadwick et al. 2013).

***D/H* ratios, water contents, and the oxidation states of Fe**

The *H* isotope compositions of core and rim samples of a set of selected amphibole megacrysts are reported in Table 3 together with their H₂O wt% and relative proportion of ferric iron (Fe³⁺/Fe_{tot}). The full set of Mössbauer parameters and the measured relative proportions of ferrous iron in these samples are provided in the online supplementary material (Appendix 3). The amphibole megacrysts record a range of δD values from -11 to -107‰ (Table 3). Core samples ($n=18$) show values from -20 to -107‰ , while rim samples ($n=18$) yield a range from -11 to -105‰ . Of the full δD data set, 17 analyses plot above the range of common igneous amphiboles, 18 plot within this range, and 4 plot below it (Fig. 3). The water contents of some amphibole samples are close to the stoichiometric amount (~ 2.1 wt%), but are lower in others (lowermost H₂O = 1.5 wt%). Megacrysts that have different water concentrations in the core and rim typically contain less water in the rim. The proportion of Fe³⁺ in these samples is variable and is overall high (47–75%); however, there seems to be no systematic variation in Fe³⁺/Fe_{tot} between the cores and rims of the sampled crystals.

Discussion

Relationship between the amphibole megacrysts and their host magmas

The similarity between the Sr and Nd isotope compositions of the amphibole megacrysts and the Merapi high-*K* basaltic andesite magmas indicates that the megacrysts are genetically linked to their host magmas, rather than being xenocrysts. As the amphibole megacrysts are in apparent textural disequilibrium with their host magmas, they may be considered antecrysts to the eruptives. Evidently, after becoming entrained in their host magmas, the amphibole megacrysts were erupted sufficiently rapidly to prevent complete dissolution to occur.

Amphibole formulas and barometry calculations

To estimate the crystallisation pressures of the amphibole megacrysts, we calculated amphibole formulas from the available EMP data according to the stoichiometric considerations of Hawthorne et al. (2012) and Locock (2014). It will be pointed out below that some of the amphibole megacrysts in our sample suite likely have become partially dehydrogenated. These megacrysts consequently contain an oxy-component (O²⁻) in the hydroxyl site, and likely have higher Fe³⁺/Fe²⁺ ratios than megacrysts that were unaffected by this process. Some megacrysts may additionally have experienced partial dehydration, a process that may be associated with the incorporation of external halogens or O²⁻ at the hydroxyl site and, in the latter case, the oxidation of structural Fe²⁺. To accurately calculate the formulas of the amphibole megacrysts, major elements, the halogens, H₂O, as well as Fe³⁺/Fe²⁺ ratios must, therefore, be known. First, F and Cl concentrations are not available for the megacrysts in our data set. Second, for practical reasons, the EMP analyses of the amphibole megacrysts were performed on different amphibole specimens than those on which the FTIR spectroscopy and Mössbauer spectroscopy measurements were done. We, therefore, calculated two sets of amphibole formulas to obtain a range of amphibole compositions: one for the likely maximum and another for the likely minimum oxy-components in the amphibole megacrysts. The maximum likely oxy-component was estimated from the lowermost H₂O wt% sample in the IR-data set (i.e., 1.5 wt% H₂O) together with the lowest values for Cl and F wt% in megacrysts from an unpublished data set on the 1998 eruptives (EMPA: F = 0.22–0.49 wt%, Cl = 0.02–0.17 wt%, $n=59$. L.M. Schwarzkopf, pers. comm). The minimum likely oxy-component is considered to be zero, i.e., the case when the amphibole megacrysts did not experience dehydrogenation and/or dehydration and, therefore, (OH + Cl + F) = 2.0 apfu. For both sets of

Table 3 δD values, H₂O wt%, and Mössbauer parameters of Merapi amphiboles megacrysts

Eruption year	Core			Rim		
	δD [‰]	H ₂ O [wt%]	Fe ³⁺ /Fe _{tot} [%]	δD [‰]	H ₂ O [wt%]	Fe ³⁺ /Fe _{tot} [%]
1994						
MP94-101	−63			−70		
MP94-102	−54	2.18		−56	2.50	
					2.10	
MP94-114	−44			−53		
MP94-162	−69			−58		
1998						
MP98-100	−20	1.53	75.1 ^a	−17		
MP98-101	−34	2.19	56.5 ^b	−36	2.11	67.4 ^b
			53.2 ^a		2.24	
MP98-103	−40	1.94	61.4 ^b	−77	1.46	53.5 ^b
		1.89	66.5 ^a			
MP98-105	−86	2.17	51.5 ^b	−80	1.86	46.9 ^b
MP98-109	−90			−88		
MP98-201	−107			−105		
MP98-202	−59			−45		
MP98-203	−88			−69		
MP98-204	−48			−44		
MP98-205	−74			−62		
MP98-206	−56			−11		
MP98-207	−93			−101		
MP98-208	−42			−51		
Merap-1A					1.89	61.7 ^a
2006						
MP2006-1	−65			−48		
	−58 (mid)					
MP2006-2	−41 (bulk)					
MP2006-3	−35 (bulk)					

Precisions of the δD values and Fe³⁺/Fe_{tot} percentages are $\pm 3\%$ and $\pm 1\%$, respectively. The H₂O wt% for core and rim is reported with $\pm 10\%$ uncertainty in precision. Mössbauer parameters are given in the supplementary materials.

^aAnalysis with standard ⁵⁷Co source

^bAnalysis with point source

amphibole formulas, the Fe³⁺/Fe²⁺ ratios were then estimated by charge balancing using the set of four cation normalisation schemes proposed by Hawthorne et al. (2012) and Locock (2014). Amphibole formulas were also calculated exclusively on the basis of the traditional 13 and 15 cations normalisation schemes (Leake et al. 1997).

Three different empirical barometers were then employed to estimate amphibole crystallisation pressures. First, we applied the barometer by Krawczynski et al. (2012), which is based on the amount of octahedrally coordinated Al (^{VI}Al) in amphibole. This barometer is expected to give the most robust results with respect to the effects of dehydrogenation and/or dehydration, because the calculated ^{VI}Al apfu in amphibole does not change with the assumed oxy-component. The hygrometer–barometer for the first

appearance of amphibole by Krawczynski et al. (2012), which is based on the magnesium number (Mg# = 100Mg/[Mg + Fe²⁺]) of the most Mg-rich amphiboles of a given sample suite, was also tested for apparently pristine domains of the amphibole megacrysts. The results of this barometer are, however, expected to overestimate crystallisation pressures of dehydrogenated and/or dehydrated megacrysts, because the oxidation of Fe²⁺ has increased their Mg#. This hygrometer–barometer was applied to the ~10% most Mg-rich amphibole compositions in our data set. As this hygrometer–barometer also depends on oxygen fugacity, p_{H₂O} was calculated with the entire spectrum of oxygen fugacity of the Merapi magmas, i.e., from 0.1 log units below the nickel–nickel oxide (NNO) buffer to 1.5 log units above it (cf., Gertisser 2001). Finally, amphibole

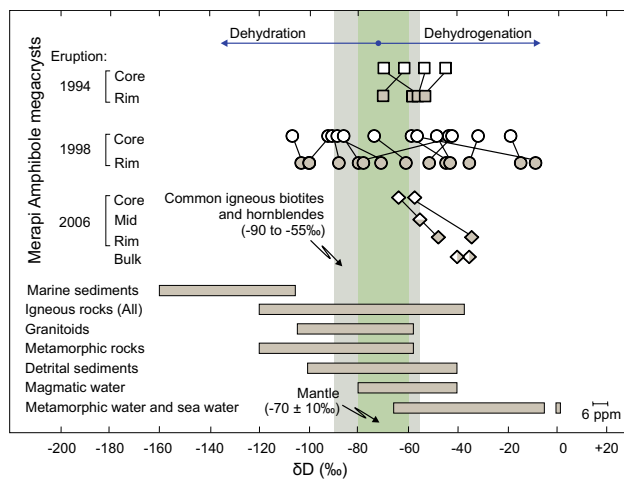


Fig. 3 Hydrogen isotope bar chart. The diagram marks well-established reference fields (after Hoefs 1997; Rollinson 1993), including the ranges of mantle rocks and that of common igneous biotites and hornblendes (vertical bars). The Merapi amphibole megacryst data notably exceed these two ranges, with an overall tendency towards higher δD values recorded in our samples. Different symbols correspond to different eruptions. Open symbols representing core samples, closed symbols representing rim samples, and mixed samples representing either intermediate or bulk samples

crystallisation depths were calculated using the barometer by Ridolfi and Renzulli (2012), which is based on the major cation composition of amphibole. This barometer was only applied to amphibole formulas that were based on the 13 cations normalisation scheme, because this method was calibrated this way (see Ridolfi et al. 2010).

The calculated amphibole crystallisation pressures are listed together with the corresponding amphibole formulas in the online supporting materials, and are shown for one megacryst in Table 4 as an example. The calculated crystallisation pressures are also shown in Fig. 4a for apparently pristine domains of the amphibole megacrysts, and in Fig. 4b for amphibole in reaction zones. According to the ^{VI}Al -based barometer by Krawczynski et al. (2012), the amphibole megacrysts crystallised at a pressure range of 524 to 895 ± 111 MPa. According to the Mg#-based hygrometer–barometer, the minimum likely range of amphibole crystallisation pressures (i.e., based on the minimum likely oxy-component of the megacrysts) is 460 to 653 ± 93 MPa for $\Delta NNO = +1.5$ and 651 to 812 ± 93 MPa for $\Delta NNO = -0.1$ and is in reasonably good agreement with the ^{VI}Al - and Mg#-based barometers are on average lower than the pressure range derived from the Ridolfi and Renzulli (2012) barometer i.e., 807 ± 93 to 1231 ± 142 MPa. We, therefore, conclude that the amphibole megacrysts formed at a minimum pressure of 500 MPa. An upper limit for the pressure of amphibole crystallisation is independently constrained

by the apparent absence of magmatic garnet in the Merapi feeding system, as is evident from REE systematics (Wulaningsih et al. 2013). Garnet is furthermore absent in plutonic xenoliths that contain amphibole (Chadwick et al. 2013), but it may be a stable phase in hydrous magmas at $P \geq 800$ MPa (e.g., Alonso-Perez et al. 2009; Jagoutz et al. 2011). We, therefore, conclude that the amphibole megacrysts crystallised at an approximate pressure range of 500 a to 800 MPa.

The calculated crystallisation pressures for amphibole in reaction zones are lower than those for the pristine domains of the amphibole megacrysts. These range from 496 to 183 ± 111 MPa (^{VI}Al -based, Krawczynski et al. 2012) and from 374 ± 43 to 659 ± 76 MPa (Ridolfi and Renzulli 2012). The lower reaction zone values likely reflect partial recrystallisation of the amphibole megacrysts during ascent.

Origin of the amphibole megacrysts in the volcanic plumbing system

At pressures of 500 and 800 MPa, amphibole is expected to be stable in hydrous arc magmas at temperatures below ca. 1000 and 1050 °C, respectively (e.g., Blatter et al. 2013; Nandedkar et al. 2014). According to the concentrations of Si, Al, Ca, Mn, and Na, i.e., temperature-sensitive elements, in experimental amphibole by Nandedkar et al. (2014), the amphibole megacrysts at Merapi crystallised at ca. 950–1030 °C (online supplementary materials, Appendix 4), i.e., in reasonable agreement with expected temperatures from the pressure calculations. Notably, concentrations of K in the amphibole megacrysts from Merapi are up to three times higher than expected from the experimental amphiboles by Nandedkar et al. (2014) at 1000 °C, likely reflecting enrichment of K in the parental magmas of the megacrysts compared to the starting materials of their experiments. The relatively high-K concentrations in the amphibole megacrysts support that the megacrysts are antecrysts to the recent high-K eruptives at Merapi.

The structure of the Merapi subsurface has been assumed as follows: A 2 km-thick low-density top layer (average density: 2242 kg m^{-3} ; Tiede et al. 2005) that overlies a “quasi-continental crust” (i.e., immature arc crust) with a density of $\sim 2660 \text{ kg m}^{-3}$ (Untung et al. 1978). The crust-mantle boundary then lies at 32–34 km below Merapi’s summit (Wölbern and Rümpler 2016). Using this profile and a minimum crystallisation pressure of ~ 500 MPa, it is calculated that the amphibole megacrysts crystallised at a minimum depth of ~ 19 km below the volcano’s summit. The higher crystallisation pressures recorded by the majority of the amphibole megacrysts suggest that amphibole crystallisation may extend down to just above the garnet stability field, i.e., at up to ~ 32 km underneath the summit. The amphibole

Table 4 Amphibole formulas and corresponding crystallisation pressures of a representative megacryst sample (Merap-1A) according to different normalisation procedures of the major cations

	4 Cation normalisation schemes			
	(OH+F+Cl)=2 apfu	Minimum H ₂ O, Cl, F wt% ^a	13eCNK	15eNK
<i>T</i>				
Si	5.932	5.932	5.961	5.947
Al	2.068	2.068	2.084	2.053
Σ <i>T</i>	8.000	8.000	8.000	8.000
<i>C</i>				
Ti	0.224	0.224	0.224	0.225
Al	0.448	0.448	0.426	0.469
Cr	0.003	0.003	0.003	0.003
Fe ³⁺	0.368	0.817	0.486	0.251
Mn ²⁺	0	0	0.016	0
Fe ²⁺	1.084	0.636	0.98	1.172
Mg	2.872	2.872	2.865	2.880
Σ <i>C</i>	5.000	5.000	5.000	5.000
<i>B</i>				
Mn ²⁺	0.016	0.016	0	0.016
Fe ²⁺	0.017	0.017	0	0.051
Ca	1.928	1.928	1.923	1.933
Na	0.039	0.039	0.077	0
Σ <i>B</i>	2.000	2.000	2.000	2.000
<i>A</i>				
Na	0.615	0.615	0.575	0.656
K	0.224	0.224	0.223	0.224
Σ <i>A</i>	0.839	0.839	0.798	0.880
<i>W</i>				
OH	n/a	1.478	n/a	n/a
F	n/a	0.103	n/a	n/a
Cl	n/a	0.005	n/a	n/a
O	n/a	0.414	n/a	n/a
Σ <i>W</i>	2.000	2.000		
Species	Pargasite	Mg-hastingsite	Mg-hastingsite	Pargasite
Crystallisation pressures [MPa]				
Ridolfi and Renzulli (2012)	n/a	n/a	918	n/a
Krawczynski et al. (2012) (^{VI} Al)	702	702	666	738
Krawczynski et al. (2012) (Mg#) ΔNNO=-0.1	755	659	169	Mg# <74
Krawczynski et al. (2012) (Mg#) ΔNNO=1.5	608	527	154	Mg# <74

Amphibole formulas of other megacryst samples are presented in the online supplements. Normalisation procedures are based on Hawthorne et al. (2012) and Locock (2014) (4 cation normalisation schemes) and Leake et al. (1997) (13eCNK and 15eNK). EMP data for this particular sample are also listed in Table 1

^aH₂O, Cl, and F contents were not determined for this particular sample, but the lowest values from the available H₂O data (H₂O > 1.5 wt%) and from an additional data set that includes Cl and F data (Cl > 0.02 wt%; F > 0.22 wt%; L.M. Schwarzkopf, pers. comm.) were considered to obtain a maximum likely oxy-component. See text for details

megacrysts thus predominantly crystallised in the mid-to-lower crust and down to the crust-mantle boundary, and are hence amongst the deepest mineral phases from the plumbing system of the volcano. Given their large crystal sizes of up to ~8 cm, they likely were derived from mafic cumulates at these depths.

The Sr isotope compositions of the amphibole megacrysts provide independent evidence for their deep origin. The range of ⁸⁷Sr/⁸⁶Sr in the megacrysts is slightly lower than that of the recent Merapi whole rock compositions, and is significantly lower than the available groundmass and plagioclase data (Gertisser and Keller 2003; Chadwick

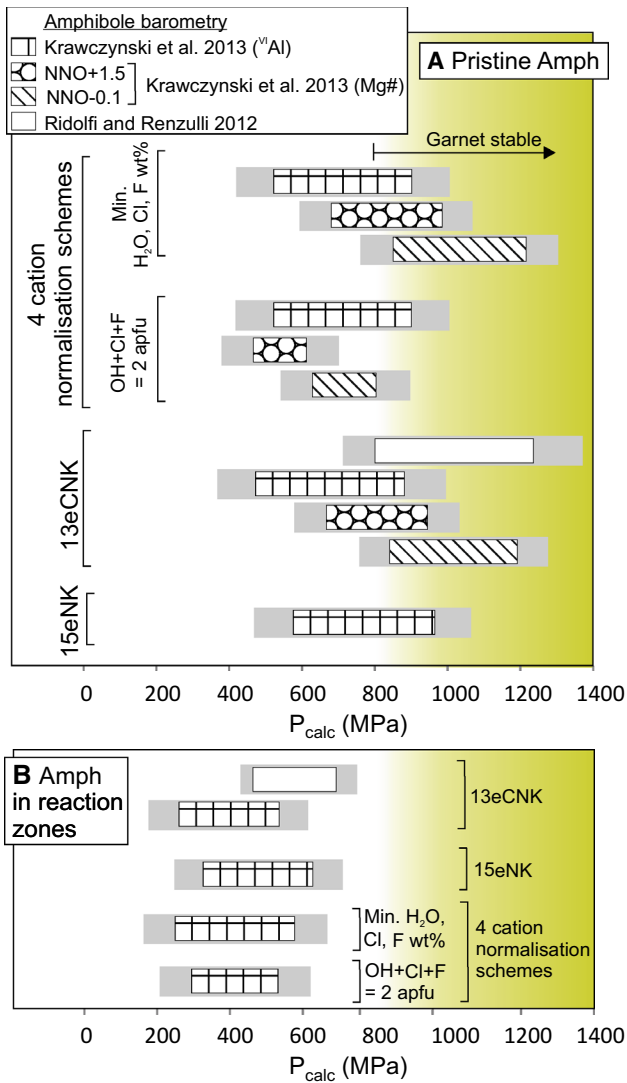


Fig. 4 Ranges of crystallisation pressures for apparently pristine domains of the amphibole megacrysts (a) and amphibole in reaction zones (b). Pressures are calculated using the indicated barometers after normalisation of the major cations. The most reliable method is based on four combined cation normalisation schemes (Hawthorne et al. 2012; Locock 2014). For this scheme, the calculated crystallisation pressures are lowest when the oxy-component is presumed to be zero (i.e., OH+F+Cl=2.0 apfu), which constrains the minimum likely crystallisation pressure of the amphibole megacrysts to approximately 500 MPa. The stability of garnet, which appears to be an absent phase in the Merapi plumbing system, constrains the upper limit of amphibole crystallisation pressures at approximately 800 MPa (cf., Alonso-Perez et al. 2009; Jagoutz et al. 2011). Calculated pressures are also shown for the traditional 15eNK and 13eCNK normalisation schemes (Leake et al. 1997) for comparison. The barometer by Ridolfi and Renzulli (2012) was only applied to amphibole formulas that were based on the traditional 13 cations normalisation scheme, in line with the calibration of this specific barometer (see Ridolfi et al. 2010)

et al. 2007, 2013). Variations in $^{87}\text{Sr}/^{86}\text{Sr}$ ratios amongst the different zones of single plagioclase crystals have been attributed to crystal growth during assimilation of

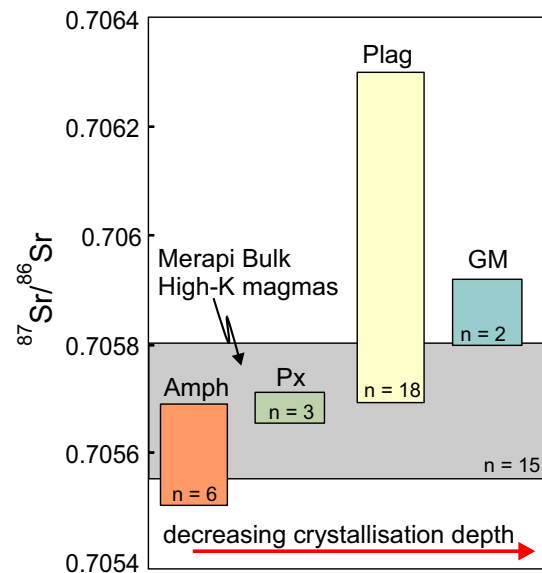


Fig. 5 Plot of $^{87}\text{Sr}/^{86}\text{Sr}$ ratios of individual components of the Merapi high-K basaltic andesite magmas compared to the bulk rock composition. Sr isotope ratios of minerals become more radiogenic with presumed decreasing crystallisation depth of the mineral phases (e.g., Chadwick et al. 2013). Amph amphibole, Px pyroxene, Plag plagioclase, GM groundmass. Pyroxene data are from Jolis (2013); plagioclase and groundmass data are from Chadwick et al. 2007; bulk composition of the high-K basaltic andesite magmas is from Gertisser and Keller (2003) and Jolis (2013)

carbonate rocks in the upper crust (≤ 10 km). The elevated whole-rock and plagioclase Sr isotope ratios relative to the amphibole megacrysts are, therefore, an indication of mixing with upper crustal materials, and thus the amphibole megacrysts likely pre-date crystallisation in the shallower levels of the Merapi magma feeding system (Fig. 5). This realisation is consistent with the lower $^{87}\text{Sr}/^{86}\text{Sr}$ ratios of clinopyroxene compared to plagioclase at Merapi (Chadwick et al. 2013; Jolis 2013), suggesting that clinopyroxene also grew dominantly prior to the onset of shallow-level sediment assimilation in the top ~10 km of the crust, which is furthermore in agreement with the oxygen isotope record for these two phases (Troll et al. 2013).

Role of amphibole fractionation in magmatic differentiation of the high-K basaltic andesite magma suite

The recent magmas that erupted at Merapi show apparently decreasing Dy/Yb and increasing La/Yb with SiO₂ wt%, suggesting that fractionation of plutonic amphibole may have played a role in the differentiation of these magmas (Wulaningsih et al. 2013). To further test this hypothesis, we have calculated the REE concentrations of the parental magma from which the amphibole megacrysts crystallised

from their average composition, using selected partition coefficients for REE between magnesiohastingsite (sample 81T116 by Sisson 1994) or pargasite (experiment “RN8 inner” by Nandedkar et al. 2016) and calc-alkaline basaltic andesite (Table 5). Given the high concentrations of *K* in the amphibole megacrysts, we also calculated REE concentrations in the amphibole megacrysts’ parent magmas using partition coefficients between magnesiohastingsite and alkaline trachybasalt (Viccaro et al. 2007) and kaersutite and alkaline basalt (Irving and Frey 1984) for comparison. The purpose of this exercise is to compare the Dy/Yb and La/Yb ratios of liquids that may have been in equilibrium with the amphibole megacrysts with the Dy/Yb and La/Yb ratios in the most primitive magmas erupted at Merapi (Fig. 6). The calculated Dy/Yb and La/Yb of the potential amphibole megacrysts’ parent magmas vary between 1.8–2.8 and 4.1–14.8, respectively, and are higher and lower than Dy/Yb and La/Yb in the most primitive erupted magma of the recent Merapi high-*K* basaltic andesite series (Dy/Yb = 1.7; La/Yb = 8.6, Gertisser and Keller 2003). In fact, the concave patterns in Fig. 6 indicate that relative to the most primitive erupted Merapi magma, the amphibole megacrysts’ parent magmas were likely enriched in REE in the mass range Gd–Er relative to the heavier REE. Moreover, relative to this most primitive erupted magma, the

heavy REE in the amphibole megacrysts’ parent magmas were likely enriched over the light REE. This conclusion suggests that magmatic differentiation at Merapi involved the fractionation of a phase that preferentially incorporated REE in the mass range Gd–Er relative to the heavier REE, and also incorporated the heavier REE preferentially to the light REE. This phase may be present as amphibole in the deep portions of the plumbing system of the volcano. In addition, substantial fractionation of clinopyroxene could explain the patterns in Fig. 6.

To further test the hypothesis that the Merapi magmas evolved by amphibole fractionation, we investigated apparently coupled trace element variations between the amphibole megacrysts. Notably, the Dy/Yb ratio of the megacrysts decreases with their La/Yb ratio (Fig. 7a). The parent magmas of the amphibole megacrysts may, therefore, have evolved towards lower Dy/Yb by progressive fractionation of amphibole and/or clinopyroxene. In addition, Zr/Hf in the amphibole megacrysts decreases with Dy/Yb (Fig. 7b), again suggesting that the deep magmas at Merapi may have evolved by progressive fractionation of amphibole and/or clinopyroxene, because these phases preferentially incorporate Hf relative to Zr (e.g., Tiepolo et al. 2001). Moreover, the concentrations of La (i.e., likely an incompatible element in the amphibole

Table 5 REE concentrations in the amphibole megacrysts’ parent magma compared to the most primitive erupted high-*K* basaltic andesite magma

	Amphibole mean [ppm]	Amphibole parent magma ^a [ppm]				Primitive high- <i>K</i> magma [ppm]
		Sisson (1994)	Nandedkar et al. (2016)	Irving and Frey (1984)	Viccaro et al. (2007)	
La	1.84	11.48	19.13	10.80	5.02	17.3
Ce	6.43	21.44	34.96	24.74	9.59	34.6
Pr	1.30	n.d.	n.d.	n.d.	1.36	4.28
Nd	8.17	10.60	16.91	18.56	6.64	18.0
Sm	3.26	2.76	3.83	4.29	2.12	4.33
Eu	1.13	n.d.	1.12	1.28	0.68	1.36
Gd	4.13	n.d.	3.46	4.81	3.09	3.65
Tb	0.65	n.d.	0.50	0.78	0.41	0.627
Dy	3.99	2.62	2.74	5.11	2.67	3.45
Ho	0.77	n.d.	0.55	n.d.	0.46	0.72
Er	2.02	1.40	1.45	2.97	1.58	1.93
Tm	0.27	n.d.	0.20	n.d.	0.21	0.318
Yb	1.52	1.48	1.29	2.58	1.22	2.01
Lu	0.21	n.d.	0.19	0.41	0.16	0.330
Dy/Yb	2.62	1.77	2.12	1.98	2.19	1.72
La/Yb	1.21	7.76	14.8	4.19	4.11	8.61

^aCalculated from the mean REE concentrations in the amphibole megacrysts and partition coefficients between magnesiohastingsite (Sisson 1994, sample 81T116) or pargasite (Nandedkar et al. 2016, experiment RN8 inner) and calc-alkaline basaltic andesite. For comparison, amphibole parent magma compositions were also calculated from partition coefficients between kaersutite and alkaline basalt (Irving and Frey 1984) and between pargasite and alkaline trachybasalt (Viccaro et al. 2007). Data for the most primitive high-*K* magma that erupted at Merapi (51.85 wt% SiO₂) were taken from Gertisser and Keller (2003). See text for details

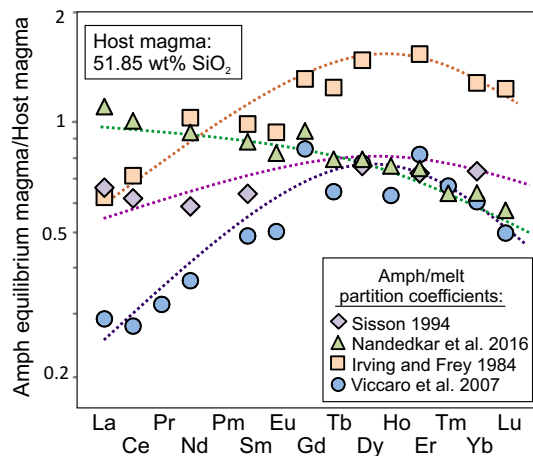


Fig. 6 Calculated concentrations of REE in the parental magmas of the amphibole megacrysts (“Amph equilibrium magma”) divided by the most primitive magma composition known from the recent eruptive series at Merapi (“Host magma”). The REE concentrations were calculated using amphibole–melt partition coefficients for calc-alkaline systems (sample 81T116 by Sisson 1994; experiment RN8 inner by; Nandedkar et al. 2016) and for alkaline systems for comparison (Irving and Frey 1984; Viccaro et al. 2007). Data for the most primitive erupted Merapi magma (51.85 wt% SiO₂) were taken from Gertisser and Keller (2003). Curves are fitted by eye for comparison. Note that patterns are typically concave rather than flat, suggesting that the amphibole host magmas had fractionated a phase that preferentially incorporated REE in the mass range Gd–Er, i.e., most likely amphibole and/or clinopyroxene, relative to the amphibole equilibrium magmas

megacrysts) apparently decrease with Dy/Yb, whereas the concentration of Dy increases (possibly a compatible element in the amphibole megacrysts; e.g., Davidson et al. 2007 and references therein), with the exception of sample MP98-2-B (Fig. 7c, d). The suggestion that Dy possibly behaved as a compatible element in the amphibole megacrysts during fractional crystallisation is in agreement with the calculated higher Dy concentrations of the amphibole megacrysts’ parent magmas relative to the most primitive high-*K* magma (3.99 and 3.45 ppm, respectively; Table 3). Importantly, Dy typically behaves as an incompatible element during fractional crystallisation of clinopyroxene in calc-alkaline basaltic magmas. The increase of Dy concentrations with Dy/Yb ratios in the amphibole megacrysts, therefore, suggests that differentiation of the deep magmas at Merapi was dominated by the fractionation of amphibole rather than clinopyroxene. Finally, Ti concentrations in the amphibole megacrysts broadly correlate with their Dy/Yb ratios too (Fig. 7e), suggesting that the deep magmas at Merapi evolved towards lower Ti concentrations by fractional crystallisation of amphibole. Indeed, in pristine domains of the amphibole megacrysts, Ti concentrations are typically

higher (>1.3 wt% TiO₂) than in the high-*K* basaltic andesite host magma (<0.9 wt% TiO₂), suggesting that Ti is likely compatible in Merapi amphibole during fractional crystallisation.

We note that some of the apparent trends in Fig. 7 may alternatively be caused by systematic differences in element partitioning behaviour with e.g., changing amphibole composition or crystallisation pressure or temperature. We, therefore, compared partition coefficients for La, Dy, and Yb between pargasite or magnesiohastingsite and melt for a wide range of systems (Irving and Frey 1984; Sisson 1994; Bottazzi et al. 1999; Tiepolo et al. 2000; Downes et al. 2004; Viccaro et al. 2007), but no systematic relation between $D_{\text{Dy/Yb}}$ and $D_{\text{La/Yb}}$ was observed (online supplementary materials, Appendix 5), rendering deep amphibole fractionation as a likely explanation for the observed trends.

To better assess the role of amphibole fractionation in magmatic differentiation of the high-*K* basaltic andesite magma suite, we modelled the evolution of Dy/Yb versus SiO₂ wt% for the most primitive magma that erupted at Merapi, assuming the extreme scenario in which amphibole was the only fractionating phase. Figure 8a shows that <30% amphibole fractionation from the most primitive erupted magma could have accounted for the observed Dy/Yb and SiO₂ wt% in the more evolved magmas. For the composition of amphibole in this model, we used the lowest Dy/Yb ratio and highest SiO₂ wt% value from amphibole megacrysts in our data set to approximate the most evolved type of amphibole at Merapi. If the highest Dy/Yb and lowest SiO₂ wt% values from our data set are used instead, i.e., an approximation of the most primitive amphibole in the Merapi system, the model curve does not significantly change (Fig. 8a).

We also modelled the differentiation by amphibole fractionation of a hypothetical primitive magma with 47.5 wt% SiO₂ and variable Dy/Yb as well as Dy and Yb concentrations. Figure 8b shows that <60% amphibole fractionation from this hypothetical primitive magma could have produced the entire ranges in Dy/Yb and SiO₂ wt% of the erupted rocks at Merapi if the primitive magma had Dy/Yb = 2.0–2.1. This range of Dy/Yb ratios is well within the range that is expected for arc magmas before amphibole fractionation, which may have Dy/Yb ratios between ~1.6 and ~2.4 (Davidson et al. 2007). Although these results seemingly underline the relevance of amphibole fractionation in magmatic differentiation processes at Merapi, we stress that other phases in addition to amphibole, notably clinopyroxene, were likely also stable at depth. Fractionation of clinopyroxene may have produced similar trends in Dy/Yb versus SiO₂ space, and the quantitative estimates above for amphibole fractionation at Merapi, therefore, likely reflect upper limits only.

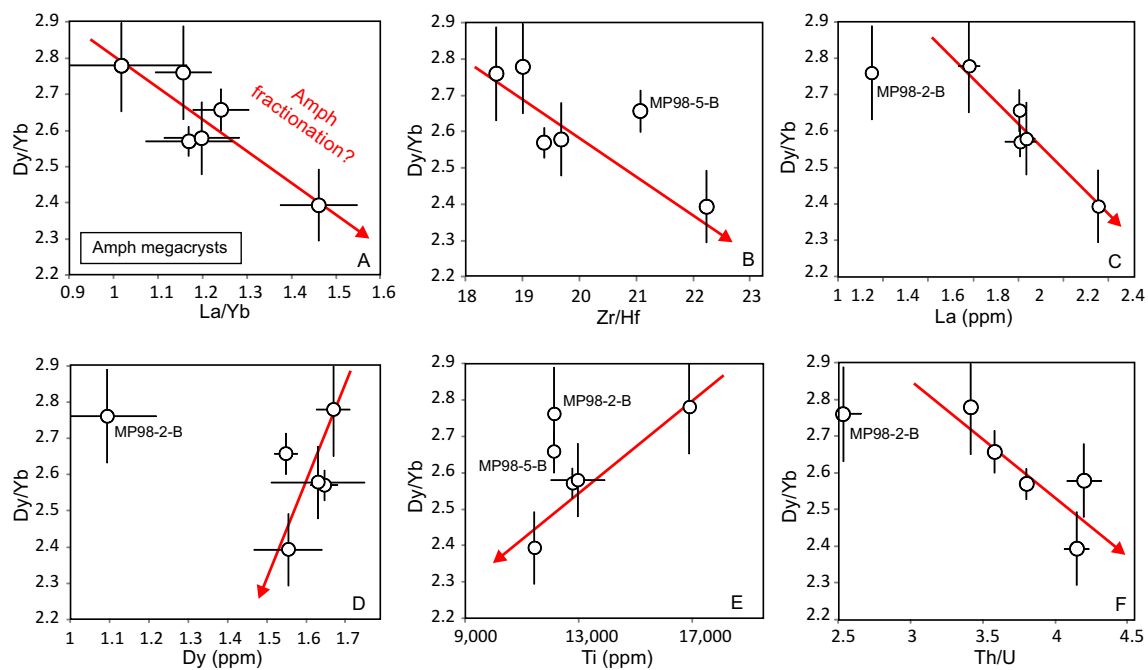


Fig. 7 Variations in trace element ratios and concentrations in selected Merapi amphibole megacrysts, possibly reflecting progressive fractionation of amphibole from the megacrysts' parent magmas. One particular sample off the trends defined by the other megacrysts for some parameters (MP98-2-B; indicated). In addition, the

Ti concentration and Zr/Hf ratios of megacryst MP98-5-B (indicated) may be affected by micro-inclusions of Fe-Ti oxides, as this sample has an unusually low Nb/Ti ratio for amphibole of ca. 0.4 (Table 2) (see text for details)

Amphibole megacrysts as a probe into the deep volcanic plumbing system

Interestingly, the Th/U ratios in the amphibole megacrysts appear to generally decrease with increasing Dy/Yb ratios (Fig. 7f), suggesting that U was more compatible during early amphibole fractionation than Th, i.e., the case when both elements occur as tetravalent cations (e.g., Tiepolo et al. 2000). The magmas that erupted at Merapi, however, range in their fO_2 from 0.6 to 2.2 log units above the FMQ buffer (Gertisser 2001). At these levels of fO_2 , U occurs predominantly in the hexavalent oxidation state and is, therefore, less compatible than Th during fractional crystallisation, which exclusively occurs in tetravalent state (e.g., Fonseca et al. 2014). Moreover, the basaltic andesite host rocks have higher Th/U (Th/U = 4.48–6.04) than the amphibole megacrysts (Th/U = 2.53–4.20), but fractional crystallisation of the major rock phases above the FMQ buffer would have decreased Th/U ratios of the residual magmas. It is, therefore, possible that the amphibole megacrysts crystallised from magmas with fO_2 below the FMQ buffer (Fonseca et al. 2014), in which case the deep magmas at Merapi are considerably more reduced than the magmas that eventually erupt at the surface. This suggestion is in agreement with the view held from Zn/Fe systematics that the typically high fO_2 levels of arc magmas (e.g., Ballhaus

1993) have at least partially originated from shallow-level differentiation processes (Lee et al. 2010). Given the common breakdown features seen with the Merapi amphibole megacrysts, the loss of H_2 by amphibole dehydrogenation above the amphibole stability field would have helped to oxidise the magmas at shallow crustal levels.

Origin of H isotope variability

The range of δD values in the amphibole megacrysts (-11 to -107%) considerably exceeds the mantle range (ca. $\delta D = -70 \pm 10$) and the range of “common igneous hornblendes and biotites” ($\delta D = -90$ to -55% ; Hoefs 1997; Rollinson 1993), and some amphibole megacrysts contain less H_2O than typical pristine amphibole (~ 2.1 wt% H_2O) (Table 3). Some variations in δD values between the megacrysts may, therefore, have originated from amphibole dehydrogenation (H_2 -loss) or amphibole dehydration (H_2O -loss) after the megacrysts had crystallised (e.g., Demény et al. 2006). Amphibole dehydrogenation is expected to result in preferential loss of 1H relative to D (2H) due to positive solid versus gas isotope fractionation, and therefore produces an increase in δD in the crystal (e.g., Feeley and Sharp 1996). The negative charge of the resultant oxy-component (O^{2-}) at the hydroxyl site is balanced by the oxidation of Fe^{2+} and, to a lesser extent,

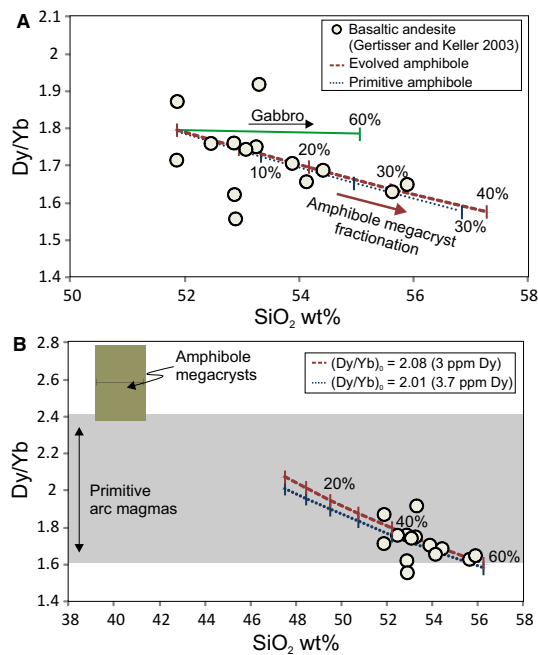


Fig. 8 Magmatic differentiation model of the Merapi magmas by fractionation of their amphibole megacrysts. Compositions of the erupted magmas are depicted by *open circles* (data from Gertisser and Keller 2003). The model curves in (a) show magmatic differentiation by amphibole fractionation of a liquid with intermediate composition to the two most primitive magmas that were erupted. Note that minor variations in the presumed amphibole composition do not significantly affect the model outcome (the *dashed* and *dotted curves* correspond to the entire compositional range of the amphibole megacrysts that were erupted at Merapi). Magmatic differentiation by fractionation of a gabbroic mineral assemblage (20% olivine, 35% clinopyroxene, 35% plagioclase) is also shown for comparison (*solid curve*). In (b) magmatic differentiation by amphibole fractionation is shown for a liquid with 47.5 wt% SiO₂. The *dotted curve* corresponds to differentiation of a magma with the maximum likely concentration of Dy before amphibole fractionation. It is assumed that this maximum likely Dy concentration equals the concentration in the most primitive magma that erupted (i.e., 3.7 ppm), because Dy behaves as a compatible element during fractional crystallisation of amphibole. Differentiation of a liquid with a more realistic starting composition (3 ppm Dy) is shown for comparison (*dashed curve*). Importantly, the Dy/Yb ratios of the primitive magmas that are required to fit the model curves through the data (i.e., Dy/Yb = 2.0–2.1) are well within the range that is expected for arc magmas before amphibole fractionation (i.e., Dy/Yb = 1.6–2.4; Davidson et al. 2007)

the oxidation of Mn²⁺ (e.g., Aoki 1963; Boettcher and O’Neil 1980; Dyar et al. 1992). Amphibole dehydration, in contrast, is expected to result in the preferential loss of D and, therefore, causes a decrease in δD in the crystal (cf., Richet et al. 1977; Dixon et al. 1991; Demény et al. 2006). After amphibole dehydration, the resultant vacancy at the hydroxyl site is likely stabilised by the incorporation of external halogen anions or O²⁻ (Demény et al. 2006). In the latter case, charge balance is likely maintained by the substitution of Fe³⁺ for Fe²⁺ (Demény et al. 2006).

In conjunction with their fluctuating water contents, two sets of observations suggest that the variable δD values of the amphibole megacrysts were caused by degassing processes. First, the amphibole samples for which Fe³⁺/Fe_{tot} and δD data are available show a general increase of δD with Fe³⁺/Fe_{tot}, as is expected for partial dehydrogenation (Fig. 9a). Second, from those amphibole megacrysts for which H isotope data for both the cores and rims are available ($n = 18$), six samples have higher δD values in the cores than in the rims. These particular megacrysts may, therefore, have degassed H₂ from the crystal rims more so than from the crystal cores. The cores of 5 megacrysts, in contrast, record lower δD values than their corresponding crystal rims. These megacrysts may have become predominantly dehydrated i.e., H₂O was lost from their rims more so than from their crystal cores.

We note that the δD and Fe³⁺/Fe_{tot} compositions of the amphibole megacrysts cannot exclusively be explained by amphibole degassing. For example, the core samples of two megacrysts (MP98-103 and MP98-105) have higher Fe³⁺/Fe_{tot} ratios than the rim samples of these megacrysts (Fig. 9a), but the H₂O contents of these samples apparently confirm that the crystal cores were less degassed than the crystal rims. This relation is not explained by amphibole dehydrogenation or with amphibole dehydration, since both processes would have increased the Fe³⁺/Fe_{tot} of the crystal rims relative to the cores. In addition, the core and rim of megacrysts sample MP98-101 have indistinguishable δD values, and also the water contents of the core and rim are apparently pristine (2.2–2.3 ± 0.2 wt% H₂O; Fig. 9b). This megacryst is, therefore, unlikely to have experienced significant degassing, but its δD values are more than 20‰ above the common igneous range. Some variability in δD values of the amphibole megacrysts may, therefore, reflect contamination during crystal growth coupled with degassing of the parent magmas from which the amphibole megacrysts crystallised.

Conclusions

Amphibole megacrysts are present in the recent high-*K* basaltic andesites of Merapi and were studied as a probe into the deeper parts of the volcanic plumbing system. Amphibole-based barometry suggests that the megacrysts in the 1994 and 1998 eruptives crystallised from primitive magmas at mid-to-lower crustal depths (ca. 500–800 MPa), in agreement with their Sr isotope compositions that indicate crystallisation prior to carbonate assimilation in the upper crust. In conjunction with the low Th/U ratios of the amphibole megacrysts relative to their host magmas, this conclusion suggests that the mid-to-lower crustal magmas at Merapi were possibly

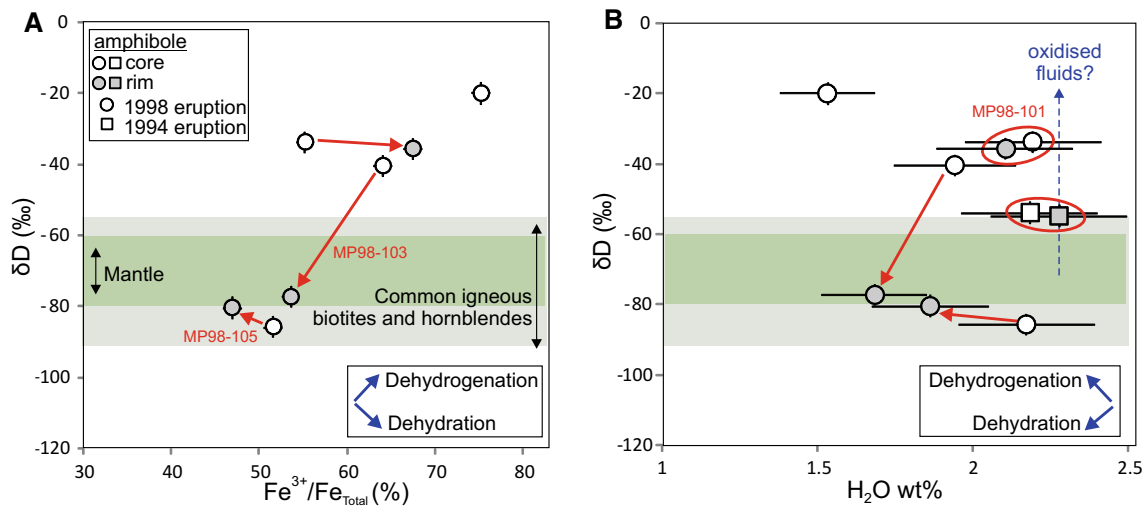


Fig. 9 Relation between δD and Fe^{3+}/Fe_{tot} ratios (a) and δD versus H_2O wt% (b) in amphibole megacrysts. Analyses of the cores and rims from single megacrysts are connected by arrows. The expected effects of dehydrogenation and dehydration on amphibole compositions are qualitatively indicated in the bottom right of the panels (after Demény et al. 2006). The δD values generally increase with Fe^{3+}/Fe_{tot} , suggesting that the amphibole megacrysts were more affected by dehydrogenation than by dehydration, but neither of these

processes can explain the lower Fe^{3+}/Fe_{tot} ratios in the rims of the two indicated megacrysts compared to their crystal cores. Note that the δD values from the core and rim of megacrysts MP98-101 are above the common igneous range, but are apparently unaffected by amphibole degassing. These observations possibly hint towards contamination of the amphibole megacrysts' parent magmas by oxidising fluids with high δD values

at considerably lower fO_2 (i.e., below the FMQ buffer) than the erupted magmas (i.e., FMQ+0.6 to +2.2). The basaltic andesite host magmas of the megacrysts seem to have fractionated significant amounts of amphibole, because they have lower Dy/Yb than the estimated compositions of the parent magmas of the megacrysts, which is also consistent with apparently coupled trace element ratios in the megacrysts. During the final stages of ascent, the amphibole megacrysts were partially resorbed by the melt, and hydrogen isotopes and H_2O concentrations imply release of volatile compounds (H_2 and H_2O) during this process. Volatile release from amphibole may be one of the explanations for Merapi's rapidly changing and at times erratic eruptive styles. In fact, the preservation of metastable amphibole megacrysts in the erupted magmas may indicate that these magmas were erupted rapidly after the onset of amphibole breakdown.

Acknowledgements We are grateful for the insightful comments by Othmar Müntener, Jon Davidson, Szabolcs Harangi, and two anonymous reviewers that helped to significantly improve the manuscript. This work furthermore benefited from discussions with John Hora, Pieter Vroon, Gareth Davies, Hans Annersten, Frances Deegan, Carsten Münker, and Sophie Omidian. We thank Henrik Skogby for his help with the IR and Mössbauer analysis. Support by the petrology department of VU University Amsterdam to S.P., the department of applied mineralogy at Erlangen to B.S., and the Swedish Science Foundation to V.R.T. (field sampling, sample preparation and D analyses) are gratefully acknowledged. In addition, S.P. and V.R.T. acknowledge financial support by the "U4" collaboration network of

the German Academic Exchange Service (DAAD), in which Göttingen and Uppsala universities are active partners.

References

- Alonso-Perez R, Müntener O, Ulmer P (2009) Igneous garnet and amphibole fractionation in the roots of island arcs: experimental constraints on andesitic liquids. *Contrib Mineral Petrol* 157(4):541–558
- Aoki K (1963) The kaersutites and oxykaersutites from alkalic rocks of Japan and surrounding areas. *J Petrol* 4(2):198–210
- Ballhaus C (1993) Redox states of lithospheric and asthenospheric upper mantle. *Contrib Mineral Petrol* 114(3):331–348
- Beard JS (1986) Characteristic mineralogy of arc-related cumulate gabbros: implications for the tectonic setting of gabbroic plutons and for andesite genesis. *Geology* 14(10):848–851
- Berthommier PC, Camus G, Condomines M, Vincent PM (1990) Le merapi (centre Java): elements de chronologie d'un stratovolcan andésitique. *Comptes rendus de l'Académie des sciences. Série 2, Mécanique, Physique, Chimie, Sciences de l'univers. Sci Terre* 311(1):213–218
- Blatter DL, Sisson TW, Hankins WB (2013) Crystallization of oxidized, moderately hydrous arc basalt at mid-to lower-crustal pressures: implications for andesite genesis. *Contrib Mineral Petrol* 166(3):861–886
- Boettcher AL, O'Neil JR (1980) Stable isotope, chemical, and petrographic studies of high-pressure amphiboles and micas: evidence for metasomatism in the mantle source regions of alkali basalts and kimberlites. *Am J Sci* 280:594–621
- Borisova AY, Gurenko AA, Martel C, Kouzmanov K, Cathala A, Bohron WA, Pratomo I, Sumarti S (2016) Oxygen isotope heterogeneity of arc magma recorded in plagioclase from the 2010

- Merapi eruption (Central Java, Indonesia). *Geochim Cosmochim Acta* 190:13–34
- Bottazzi P, Tiepolo M, Vannucci R, Zanetti A, Brumm R, Foley SF, Oberti R (1999) Distinct site preferences for heavy and light REE in amphibole and the prediction of Amph/LDREE. *Contrib Mineral Petrol* 137(1–2):36–45
- Camus G, Gourgaud A, Mossand-Berthommier PC, Vincent PM (2000) Merapi (Central Java, Indonesia): an outline of the structural and magmatological evolution, with a special emphasis to the major pyroclastic events. *J Volcanol Geotherm Res* 100(1):139–163
- Cawthorn RG, O'Hara MJ (1976) Amphibole fractionation in calc-alkaline magma genesis. *Am J Sci* 276(3):309–329
- Chadwick JP, Troll VR, Ginibre C, Morgan D, Gertisser R, Waight TE, Davidson JP (2007) Carbonate assimilation at Merapi Volcano, Java, Indonesia: insights from crystal isotope stratigraphy. *J Petrol* 48(9):1793–1812
- Chadwick JP, Troll VR, Waight TE, van der Zwan FM, Schwarzkopf LM (2013) Petrology and geochemistry of igneous inclusions in recent Merapi deposits: a window into the sub-volcanic plumbing system. *Contrib Mineral Petrol* 165(2):259–282
- Conrad WK, Kay RW (1984) Ultramafic and mafic inclusions from Adak Island: crystallization history, and implications for the nature of primary magmas and crustal evolution in the Aleutian Arc. *J Petrol* 25(1):88–125
- Costa F, Andreastuti S, de Maisonneuve CB, Pallister JS (2013) Petrological insights into the storage conditions, and magmatic processes that yielded the centennial 2010 Merapi explosive eruption. *J Volcanol Geotherm Res* 261:209–235
- Davidson J, Turner S, Handley H, Macpherson C, Dosseto A (2007) Amphibole “sponge” in arc crust? *Geology* 35(9):787–790
- Davies GR, Stolz AJ, Mahotkin IL, Nowell GM, Pearson DG (2006) Trace element and Sr–Pb–Nd–Hf isotope evidence for ancient, fluid-dominated enrichment of the source of Aldan Shield lamproites. *J Petrol* 47(6):1119–1146
- DeBari SM, Coleman RG (1989) Examination of the deep levels of an island arc: evidence from the tonsina ultramafic-mafic assemblage, Tonsina, Alaska. *J Geophys Res Solid Earth* (1978–2012) 94(B4):4373–4391
- Debari S, Kay SM, Kay RW (1987) Ultramafic xenoliths from Adagdak volcano, Adak, Aleutian Islands, Alaska: deformed igneous cumulates from the Moho of an island arc. *J Geol* 95:329–341
- Demény A, Vennemann TW, Harangi S, Homonnay Z, Fórizs I (2006) H₂O- δ D-FeIII relations of dehydrogenation and dehydration processes in magmatic amphiboles. *Rapid Commun Mass Spectrom* 20(5):919–925
- Dixon JE, Clague DA, Stolper EM (1991) Degassing history of water, sulfur, and carbon in submarine lavas from Kilauea Volcano, Hawaii. *J Geol* 99:371–394
- Donoghue E, Troll VR, Schwarzkopf LM, Clayton G, Goodhue R (2009) Organic block coatings in block-and-ash flow deposits at Merapi Volcano, central Java. *Geol Mag* 146(01):113–120
- Downes H, Seghedi I, Szakacs A, Dobosi G, James DE, Vaselli O, Rigby IJ, Ingram GA, Rex D, Pecskey Z (1995) Petrology and geochemistry of late tertiary/quaternary mafic alkaline volcanism in Romania. *Lithos* 35(1):65–81
- Downes H, Beard A, Hinton R (2004) Natural experimental charges: an ion-microprobe study of trace element distribution coefficients in glass-rich hornblende and clinopyroxene xenoliths. *Lithos* 75(1):1–17
- Dyar MD, McGuire AV, Mackwell SJ (1992) Fe³⁺/H⁺ and D/H in kaersutites—misleading indicators of mantle source fugacities. *Geology* 20(6):565–568
- Eggs SM, Woodhead JD, Kinsley LPJ, Mortimer GE, Sylvester P, McCulloch MT, Hergt JM, Handler MR (1997) A simple method for the precise determination of ≥ 40 trace elements in geological samples by ICPMS using enriched isotope internal standardisation. *Chem Geol* 134(4):311–326
- Erdmann S, Martel C, Pichavant M, Kushnir A (2014) Amphibole as an archivist of magmatic crystallization conditions: problems, potential, and implications for inferring magma storage prior to the paroxysmal 2010 eruption of Mount Merapi, Indonesia. *Contrib Mineral Petrol* 167(6):1–23
- Feeley TC, Sharp ZD (1996) Chemical and hydrogen isotope evidence for in situ dehydrogenation of biotite in silicic magma chambers. *Geology* 24(11):1021–1024
- Foden JD, Green DH (1992) Possible role of amphibole in the origin of andesite: some experimental and natural evidence. *Contrib Mineral Petrol* 109(4):479–493
- Fonseca RO, Mallmann G, Sprung P, Sommer JE, Heuser A, Speelmanns IM, Blanchard H (2014) Redox controls on tungsten and uranium crystal/silicate melt partitioning and implications for the U/W and Th/W ratio of the lunar mantle. *Earth Planet Sci Lett* 404:1–13
- Gertisser R (2001) Gunung Merapi (Java, Indonesien): Eruptionsgeschichte und magmatische Evolution eines Hochrisiko-Vulkans. Doctoral dissertation Albert Ludwigs University of Freiburg, pp 381
- Gertisser R, Keller J (2003) Trace element and Sr, Nd, Pb and O isotope variations in medium-K and high-K volcanic rocks from Merapi Volcano, Central Java, Indonesia: evidence for the involvement of subducted sediments in Sunda Arc magma genesis. *J Petrol* 44(3):457–489
- Gertisser R, Charbonnier SJ, Keller J, Quidelleur X (2012) The geological evolution of Merapi volcano, Central Java, Indonesia. *Bull Volcanol* 74(5):1213–1233
- Hawthorne FC, Oberti R, Harlow GE, Maresch WV, Martin RF, Schumacher JC, Welch MD (2012) Nomenclature of the amphibole supergroup. *Am Mineral* 97(11–12):2031–2048
- Hoefs J (1997) Stable isotope geochemistry, 3rd edn. Springer, Heidelberg, p 241
- Hut G (1987) Consultants' group meeting on stable isotope reference samples for geochemical and hydrological investigations. IAEA, Vienna 16–18 september 1985. Report to the Director General, vol. International Atomic Energy Agency
- Irving AJ, Frey FA (1984) Trace element abundances in megacrysts and their host basalts: constraints on partition coefficients and megacryst genesis. *Geochim Cosmochim Acta* 48(6):1201–1221
- Jagoutz O, Müntener O, Schmidt MW, Burg JP (2011) The roles of flux- and decompression melting and their respective fractionation lines for continental crust formation: evidence from the Kohistan arc. *Earth Planet Sci Lett* 303(1):25–36
- Jolis EM (2013) Magma-Crust Interaction at Subduction Zone Volcanoes, Doctoral dissertation Acta Universitatis Upsaliensis, p 40
- Kiss B, Harangi S, Ntaflou T, Mason PR, Pál-Molnár E (2014) Amphibole perspective to unravel pre-eruptive processes and conditions in volcanic plumbing systems beneath intermediate arc volcanoes: a case study from Ciomadul volcano (SE Carpathians). *Contrib Mineral Petrol* 167(3):1–27
- Klaver M, Djuly T, de Graaf S, Sakes A, Wijbrans J, Davies G, Vroon P (2015) Temporal and spatial variations in provenance of Eastern Mediterranean sea sediments: implications for Aegean and Aeolian arc volcanism. *Geochim Cosmochim Acta* 153:149–168
- Koornneef JM, Bouman C, Schwieters JB, Davies GR (2013) Use of 10^{12} ohm current amplifiers in Sr and Nd isotope analyses by TIMS for application to sub-nanogram samples. *J Anal At Spectrom* 28(5):749–754
- Koornneef JM, Bouman C, Schwieters JB, Davies GR (2014) Measurement of small ion beams by thermal ionisation mass spectrometry using new 10^{13} Ohm resistors. *Anal Chim Acta* 819:49–55

- Krawczynski MJ, Grove TL, Behrens H (2012) Amphibole stability in primitive arc magmas: effects of temperature, H₂O content, and oxygen fugacity. *Contrib Mineral Petrol* 164(2):317–339
- Lapierre H, Ortiz LE, Abouchami W, Monod O, Coulon C, Zimmermann J-L (1992) A crustal section of an intra-oceanic island arc: the late Jurassic-Early Cretaceous Guanajuato magmatic sequence, central Mexico. *Earth Planet Sci Lett* 108(1):61–77
- Larocque J, Canil D (2010) The role of amphibole in the evolution of arc magmas and crust: the case from the Jurassic Bonanza arc section, Vancouver Island, Canada. *Contrib Mineral Petrol* 159(4):475–492
- Le Maitre RW (2002) *Igneous rocks: a classification and glossary of terms: a classification and glossary of terms: recommendations of the International Union of Geological Sciences, Subcommittee on the Systematics of Igneous Rocks*, vol. Cambridge University Press, Cambridge
- Leake BE, Woolley AR, Hawthorne FC, Kato A, Kisch HJ, Krivovichev VG, Linthout K, Laird JO, Maresch WV, Schumacher JC, Stephenson NC, Whittaker EJ (1997) Nomenclature of amphiboles: report of the subcommittee on amphiboles of the International Mineralogical Association, Commission on new minerals and mineral names. *Can Mineral* 35:219–246
- Lee CTA, Luffi P, Le Roux V, Dasgupta R, Albarède F, Leeman WP (2010) The redox state of arc mantle using Zn/Fe systematics. *Nature* 468(7324):681–685
- Locock AJ (2014) An Excel spreadsheet to classify chemical analyses of amphiboles following the IMA 2012 recommendations. *Comput Geosci* 62:1–11
- Macpherson CG, Dreher ST, Thirlwall MF (2006) Adakites without slab melting: high pressure differentiation of island arc magma, Mindanao, the Philippines. *Earth Planet Sci Lett* 243(3):581–593
- Meyer I, Davies GR, Stuu JBW (2011) Grain size control on Sr-Nd isotope provenance studies and impact on paleoclimate reconstructions: an example from deep-sea sediments offshore NW Africa. *Geochem Geophys Geosyst* 12(3). doi:10.1029/2010GC003355
- Murphy MD, Sparks RS, Barclay J, Carroll MR, Lejeune AM, Brewer TS, Macdonald R, Black S, Young S (1998) The role of magma mixing in triggering the current eruption at the Soufriere Hills Volcano, Montserrat. *Geophys Res Lett* 25(18):3433–3436
- Nadeau O, Williams-Jones AE, Stix J (2013) Magmatic-hydrothermal evolution and devolatilization beneath Merapi volcano, Indonesia. *J Volcanol Geotherm Res* 261:50–68
- Nandedkar RH, Ulmer P, Müntener O (2014) Fractional crystallization of primitive, hydrous arc magmas: an experimental study at 0.7 GPa. *Contrib Mineral Petrol* 167(6):1–27
- Nandedkar RH, Hürlimann N, Ulmer P, Müntener O (2016) Amphibole-melt trace element partitioning of fractionating calc-alkaline magmas in the lower crust: an experimental study. *Contrib Mineral Petrol* 171(8–9):71
- Newhall CG, Bronto S, Alloway B, Banks NG, Bahar I, Del Marmol MA, Hadisantono RD, Holcomb RT, McGeehin J, Miksic JN (2000) 10,000 years of explosive eruptions of Merapi Volcano, Central Java: archaeological and modern implications. *J Volcanol Geotherm Res* 100(1):9–50
- Ozima M, Larson EE (1970) Low- and high-temperature oxidation of titanomagnetite in relation to irreversible changes in the magnetic properties of submarine basalts. *J Geophys Res* 75(5):1003–1017
- Pin C, Briot D, Bassin C, Poitrasson F (1994) Concomitant separation of strontium and samarium-neodymium for isotopic analysis in silicate samples, based on specific extraction chromatography. *Anal Chim Acta* 298(2):209–217
- Preece K, Barclay J, Gertisser R, Herd RA (2013) Textural and micro-petrological variations in the eruptive products of the 2006 dome-forming eruption of Merapi volcano, Indonesia: implications for sub-surface processes. *J Volcanol Geotherm Res* 261:98–120
- Prescher C, McCammon C, Dubrovinsky L (2012) MossA: a program for analyzing energy-domain Mössbauer spectra from conventional and synchrotron sources. *J Appl Crystallogr* 45:329–331
- Raczek I, Jochum KP, Hofmann AW (2003) Neodymium and strontium isotope data for USGS reference materials BCR-1, BCR-2, BHVO-1, BHVO-2, AGV-1, AGV-2, GSP-1, GSP-2 and eight MPI-DING reference glasses. *Geostand News* 27(2):173–179
- Richet P, Bottinga Y, Janoy M (1977) A review of hydrogen, carbon, nitrogen, oxygen, sulphur, and chlorine stable isotope enrichment among gaseous molecules. *Annu Rev Earth Planet Sci* 5:65–110
- Ridolfi F, Renzulli A (2012) Calcic amphiboles in calc-alkaline and alkaline magmas: thermobarometric and chemometric empirical equations valid up to 1130 °C and 2.2 GPa. *Contrib Mineral Petrol* 163(5):877–895
- Ridolfi F, Renzulli A, Puerini M (2010) Stability and chemical equilibrium of amphibole in calc-alkaline magmas: an overview, new thermobarometric formulations and application to subduction-related volcanoes. *Contrib Mineral Petrol* 160(1):45–66
- Ringwood AE (1974) The petrological evolution of island arc systems twenty-seventh William Smith Lecture. *J Geol Soc* 130(3):183–204
- Rollinson HR (1993) *Using geochemical data: evaluation, presentation, interpretation*, vol. Longman, UK, p 352
- Romick JD, Kay SM, Kay RW (1992) The influence of amphibole fractionation on the evolution of calc-alkaline andesite and dacite tephra from the central Aleutians, Alaska. *Contrib Mineral Petrol* 112(1):101–118
- Rooney TO, Franceschi P, Hall CM (2011) Water-saturated magmas in the Panama Canal region: a precursor to adakite-like magma generation? *Contrib Mineral Petrol* 161(3):373–388
- Rutherford MJ, Hill PM (1993) Magma ascent rates from amphibole breakdown: an experimental study applied to the 1980–1986 Mount St. Helens eruptions. *J Geophys Res* 98(19):667–685
- Sharp ZD, Atudorei V, Durakiewicz T (2001) A rapid method for determination of hydrogen and oxygen isotope ratios from water and hydrous minerals. *Chem Geol* 178(1):197–210
- Sigurðsson H, Shepherd JB (1974) Amphibole-bearing basalts from the submarine volcano Kick'em-Jenny in the Lesser Antilles island arc. *Bull Volcanol* 38(3):891–910
- Sisson TW (1994) Hornblende-melt trace-element partitioning measured by ion microprobe. *Chem Geol* 117(1):331–344
- Skogby H, Rossman GR (1991) The intensity of amphibole OH bands in the infrared absorption spectrum. *Phys Chem Minerals* 18:64–68
- Stalder R, Prechtel F, Ludwig T (2012) No site-specific infrared absorption coefficients for OH-defects in pure enstatite. *Eur J Mineral* 24:465–470
- Surono, Jousset P, Pallister J, Boichu M, Buongiorno MF, Budisantoso A, Costa F, Andreastuti S, Prata F, Schneider D, Clarisse L (2012) The 2010 explosive eruption of Java's Merapi volcano—a '100-year' event. *J Volcanol Geotherm Res* 241:121–135
- Thirlwall MF (1991) Long-term reproducibility of multicollector Sr and Nd isotope ratio analysis. *Chem Geol Isotope Geosci Sect* 94(2):85–104
- Tiede C, Camacho AG, Gerstenecker C, Fernandez J, Suyanto I (2005) Modeling the density at Merapi volcano area, Indonesia, via the inverse gravimetric problem. *Geochem Geophys Geosyst* 6(9). doi:10.1029/2005GC000986
- Tiepolo M, Vannucci R, Oberti R, Foley S, Bottazzi P, Zanetti A (2000) Nb and Ta incorporation and fractionation in titanian pargasite and kaersutite: crystal-chemical constraints and implications for natural systems. *Earth Planet Sci Lett* 176(2):185–201
- Tiepolo M, Bottazzi P, Foley SF, Oberti R, Vannucci R, Zanetti A (2001) Fractionation of Nb and Ta from Zr and Hf at

- mantle depths: the role of titanian pargasite and kaersutite. *J Petrol* 42(1):221–232
- Troll VR, Hilton DR, Jolis EM, Chadwick JP, Blythe LS, Deegan FM, Schwarzkopf LM, Zimmer M (2012) Crustal CO₂ liberation during the 2006 eruption and earthquake events at Merapi volcano, Indonesia. *Geophysical Research Letters* 39(11). doi:[10.1029/2012GL051307](https://doi.org/10.1029/2012GL051307)
- Troll VR, Deegan FM, Jolis EM, Harris C, Chadwick JP, Gertisser R, Schwarzkopf LM, Borisova AY, Bindeman IN, Sumarti S (2013) Magmatic differentiation processes at Merapi Volcano: inclusion petrology and oxygen isotopes. *J Volcanol Geotherm Res* 261:38–49. doi:[10.1029/2012GL051307](https://doi.org/10.1029/2012GL051307)
- Turner S, Foden J, George R, Evans P, Varne R, Elburg M, Jenner G (2003) Rates and processes of potassic magma evolution beneath Sangeang Api volcano, East Sunda arc, Indonesia. *J Petrol* 44(3):491–515
- Untung M, Sato Y, Satou Y (1978) Gravity and geological studies in Jawa, Indonesia, vol. Geological Survey of Japan
- van Bemmelen RW (1949) The geology of Indonesia, vol. General Geology Of Indonesia And Adjacent Archipelagoes
- Wölbern I, Rümpker G (2016) Crustal thickness beneath Central and East Java (Indonesia) inferred from P receiver functions. *J Asian Earth Sci* 115:69–79
- van der Zwan FM, Chadwick JP, Troll VR (2013) Textural history of recent basaltic-andesites and plutonic inclusions from Merapi volcano. *Contrib Mineral Petrol* 166(1):43–63
- Viccaro M, Ferlito C, Cristofolini R (2007) Amphibole crystallization in the Etnean feeding system: mineral chemistry and trace element partitioning between Mg-hastingsite and alkali basaltic melt. *Eur J Mineral* 19(4):499–511
- Voight B, Constantine EK, Siswoidjoyo S, Torley R (2000) Historical eruptions of Merapi volcano, central Java, Indonesia, 1768–1998. *J Volcanol Geotherm Res* 100(1):69–138
- Wulaningsih T, Humaida H, Harijoko A, Watanabe K (2013) Major element and rare earth elements investigation of Merapi Volcano, Central Java, Indonesia. *Procedia Earth Planet Sci* 6:202–211